Arabian Journal of Chemistry 16 (2023) 105228

Contents lists available at ScienceDirect

Arabian Journal of Chemistry

journal homepage: www.sciencedirect.com

Original article

High performance biobased poly(ethylene 2,5-furandicarboxylate) nanocomposites for food and cosmetics packaging materials: PMDA chain extended and TiO_2 NPs functionalized

Yuxuan Li [a,b], Yuhao Zhao [a,b], Yuze Dai [a], Ying Zhang [b,*], Min Jiang [a,*], Guangyuan Zhou [a,*]

[a] Division of Energy Materials (DNL 22), Dalian Institute of Chemical Physics, Chinese Academy of Sciences, Dalian 116023, China
[b] Laboratory of Industrial Ecology and Environmental Engineering (MOE), School of Environmental Science and Technology, Dalian University of Technology, Dalian 116024, China

ARTICLE INFO

Article history:
Received 30 May 2023
Accepted 30 August 2023
Available online 4 September 2023

Keywords:
Poly(ethylene 2,5-furandicarboxylate) (PEF)
Polymer chain extension
PEF/TiO_2 nanocomposites
Anti-ultraviolet functions
Anti-blue-light functions
Antibacterial functions

ABSTRACT

Poly (ethylene 2,5-furandicarboxylate) (PEF) has attracted more attention due to its excellent properties and great potential to be the substitute of the petroleum-based polyethylene terephthalate (PET). However, the improvement of toughness and functionality from nano materials were limited. Here, we prepared novel PEF/TiO_2 nanocomposites from dimethyl 2,5-furandicarboxylate (DMFD), ethylene glycol (EG), pyromellitic dianhydride (PMDA) and TiO_2 nanoparticles via one-pot polycondensation. The optimized PMDA (5‰ mol/mol of DMFD), TiO_2 (60 nm, 0.5-10‰ wt./wt. of PEF) or TiO_2 (30 nm or 100 nm, 3‰) served as extender, fillers, and comparison, respectively. The T_gs (~88 °C) and the thermal stability of all nanocomposites were higher than pure PEF. The crystallization rate of the nanocomposites (60 nm-TiO_2, 3‰) was improved mostly, and its half-crystallization time ($t_{1/2}$) decreased to 6.16 min at 160 °C. The impact strength of nanocomposites (60 nm-TiO_2, 10‰) could reach to 52.2 × 10^3 J/m^2. Interestingly, the ultraviolet and blue-light shielding of PEF/TiO_2 nanocomposites increased from 45.4% to 93.5% and 21.5% to 74.3%, respectively. The antibacterial activity of nanocomposites against E. coli also increased to 83%. The maximum migration of Ti during 35 d was 1.82 μg/g (FDA and EU guidance level are 10 μg/g). PEF/TiO_2 nanocomposites shown great potential in industrial production and application.

1. Introduction

In regard to the rapid consumption of fossil fuels, exploring biobased materials presented a possible solution for the sustainable development of materials (Wang et al., 2017a). Among the myriad of biobased polymers, increasing attention has been given to poly (ethylene 2,5-furandicarboxylate) (PEF) as one of the most promising candidates for poly(ethylene terephthalate) (PET) due to its structural analog of PET (Menager et al., 2018, Sousa and Silvestre, 2022). It has been reported that PEF presents superior stiffness and strength (Sousa et al., 2021), additionally, PEF has highly increased barrier properties. The barriers of O_2 and CO_2 are extensively reported to be 2–11 (Sun et al., 2019, Xie et al., 2020, Wang et al., 2017a) and 10–19 (Wang et al., 2017a, Xie et al., 2020, Wang et al., 2016) times higher than those of PET, which shows the great application potential of PEF as a kind of biobased polymer in the field of packaging. On the one hand, PEF's suitability for films and bottles is still limited due to the reasons, such as slow crystallization rate and brittle fracture (Sousa et al., 2021); on the other hand, the development of additional functional properties of PEF is also worth studying. For example, there are still benefits to exploring polyester materials to meet the requirements of packaging materials for antibacterial, anti-ultraviolet and anti-blue-light functions, etc.

Polymer nanocomposites have been synthesized with pleasing enhancement of mechanical and crystallization properties at very low filler loadings (Loos et al., 2020), due to the large specific surface area of nanosized particles. In addition, nanoparticles can endow matrix materials with some innovative properties, for example, endowing composite materials with antibacterial properties (Zhu, Cai and Sun, 2018, Zhang et al., 2022a), UV resistance properties (Hu et al., 2019a, Huang et al., 2019), becoming electrical components(Xu et al., 2019), optical components(Karthikeyan

* Corresponding authors.
E-mail addresses: yzhang@dlut.edu.cn (Y. Zhang), jiangmin@dicp.ac.cn (M. Jiang), gyzhou@dicp.ac.cn (G. Zhou).
Peer review under responsibility of King Saud University.

Production and hosting by Elsevier

https://doi.org/10.1016/j.arabjc.2023.105228
1878-5352/

et al., 2019), etc. Azarakhsh et al. prepared functional composite materials with excellent resistance to *Pseudomonas aeruginosa*, and *Escherichia coli* bacteria by doping silver nanoparticles with polyvinyl alcohol (Azarakhsh, Bahiraei and Haidari, 2022). In another study, Karthikeyan et al. introduced nano silica into polyvinyl alcohol to prepare composite materials with excellent optical properties, which could be suitable for opto-electronic applications (Karthikeyan et al., 2019). Zibaei et al. prepared antioxidant composite materials with significantly reduced water vapor permeability using polyolefin elastomers, selenium nanoparticles, and triethyl citrate (Zibaei et al., 2023). Wang et al. studied a composite material with catalytic performance, achieving excellent wastewater treatment results (Wang et al., 2023a, Wang et al., 2023b). Watte et al. investigated the preparation of anatase nanocrystal films with photocatalytic activity on a polymer substrate, and evaluated the surface morphology, transparency and photocatalytic degradation of organic pollutants of the films prepared by dipping coating(Watté et al., 2016). However, research on PEF/nanocomposites is still limited. (Xie et al., 2019) synthesized PEF/organically modified montmorillonite (OMMT) nanocomposites by melt polycondensation, and found that the melt crystallization, tensile modulus and strength were significantly improved when the addition of OMMT was 2.5 wt%. (Martino et al., 2017) designed PEF/sepiolite or OMMT nanocomposites by melt extrusion and compression molding, and found that nanocomposites with intercalated morphology presented higher thermal decomposition temperatures, and a change in T_g was observed when the amount of nanoparticles was higher. (Lotti et al., 2016) designed PEF/MWCNTs (with –COOH or $–NH_2$), or GO nanocomposites by melt polycondensation and found that the fillers acted as nucleating agents for PEF crystallization to different extents, showing a faster crystallization rate and slightly decreased thermal stability. (Codou et al., 2017) studied the effect of different extrusion parameters on PEF/cellulose nanocomposites prepared by twin-screw extrusion, and the results showed that the crystallization half time of nanocomposites could be decreased progressively with the increasing percentage of cellulose, which could be reduced by approximately 35% at most. (Achilias et al., 2017) designed PEF/TiO_2 and SiO_2 nanocomposites, and showed that the presence of the nano additives resulted in higher transesterification kinetic rate constants and lower activation energies from both the experimental measurements and the theoretical simulation. which caused a slightly higher average molecular weight of nanocomposites. (Koltsakidou et al., 2019) selected PEF as the substrate and prepared PEF/TiO_2 nanocomposites with high concentration of TiO_2 NPs (20%), as effective photocatalysts for anti-inflammatory/analgesic drugs, which was another application scenario that could be developed besides being used as a packaging material. Most of these works on PEF/-nanocomposites focused on crystallization rate, molecular weight, mechanical properties, thermal stability, etc. From the perspective of packaging material development, the innovative functions that nanoparticles can bring to the matrix, such as ultraviolet shielding, blue-light shielding, and antimicrobial, are also in urgent need of research.

Titanium dioxide could generate the unique photogenerated electron-hole pairs under light irradiation. In order to improve the photocatalytic performance of titanium dioxide, Yang et al. prepared unique Co_3O_4/TiO_2 heterojunctions serves, which produced more active radicals and holes to enhance the photothermal performance (Yang et al., 2022b, Yang et al., 2022a).Chen et al. successfully prepared uniform tablet-like TiO_2/C nanocomposites with high specific surface area by calcining MIL125(Ti) in order to degrade the tetracycline (TC) (Chen et al., 2020a). In the same year, Chen et al. prepared a novel octahedral TiO_2-MIL-101 (Cr) (T-MCr) photocatalyst with type-II heterojunction and surface heterojunction and showed the outstanding photocatalytic activity (Chen et al., 2020b). Zhang et al. performed type-II heterojunction by the encapsulation of Materials of Institut Lavoisier (MIL-101), and then the heterophase junction was further constructed to improve the catalytic performance of the photocatalyst (Zhang et al., 2022c, Zhang et al., 2022b). Titanium dioxide also exhibits excellent performance in smaller sizes, such as titanium dioxide nanoparticles (TiO_2 NPs). On the one hand, inorganic particles have better temperature resistance than organic substances (Nakazato et al., 2017); on the other hand, TiO_2 NPs have many advantages, such as biocompatibility, photocatalytic properties, high anti-ultraviolet and anti-blue-light properties, low toxicity, and antibacterial activity (Mesgari, Aalami and Sahebkar, 2021, Zhang and Rhim, 2022), and often are selected as nano fillers for polymers. Luo et al. used ultraviolet (UV) light for the directed migration of inorganic nanoparticles in a polymer film, producing an ultra-thin (100–200 nm) nanoparticle layer on the film's light-exposed surface (Luo et al., 2022). Kaur et al. prepared coating materials and titanium dioxide nanocomposites using lignin as raw materials, and coated TiO_2 nanocomposite doped lignin coating on cotton fabric, showing good antibacterial activity (Kaur et al., 2021). Bouadjela et al. developed a strong polymer dispersed liquid crystal material and investigated the dynamic expansion of polymer networks (Bouadjela et al., 2017). Sadowski et al. treated polymers (PP) with low temperature oxygen plasma, then deposited TiO_2 nanoparticles and sensitized them with organic ligands, enabling the synthesis of photocatalytic coatings with visible-induced photoactivity on the polymers (Sadowski et al., 2019). Salomatina et al. synthesized polytitanium oxide (PTO) nanocomposite copolymers using gold nanoparticles (NPs) doped polyhydroxyethyl methacrylate (HEMA) as organic matrix through a one-pot reaction (Salomatina et al., 2016). More and more studies have investigated the functions of polymer/nanocomposites doped with TiO_2 NPs. According to the literature, polyesters (such as poly (butene 2,5-furan dicarboxylate) (PBF), polylactide (PLA), cellulose triacetate (CTA), poly(propylene carbonate) (PPC) and PMMA incorporated with TiO_2 NPs maintained excellent ultraviolet shielding (Zhou et al., 2021, Gomez-Hermoso-de-Mendoza, Gutierrez and Tercjak, 2020, Wu et al., 2019, Can and Kaynak, 2020) and antibacterial properties (Zhang and Rhim, 2022, Siripatrawan and Kaewklin, 2018, Nikolic et al., 2021, Mesgari et al., 2021, Al-Tayyar, Youssef and Al-Hindi, 2020); moreover, their mechanical properties could be enhanced in a certain concentration range (Vejdan et al., 2016, Gomez-Hermoso-de-Mendoza et al., 2020). Adding TiO_2 NPs to polyester may not only change the crystallization rate, mechanical properties and thermal stability of the substrate material, but may also make polymer nanocomposites exhibit antibacterial properties and ultraviolet shielding performance due to TiO_2 NPs. Therefore, the combination of bio-based PEF with TiO_2 NPs is also promising.

However, brittle materials with inorganic rigid particles may have worse toughness (Gomez-Hermoso-de-Mendoza et al., 2020), which may require the substrate material to be a quasi-ductile material before preparing the nanocomposites. In this study, pyromellitic dianhydride (PMDA) was selected as a chain extender to prepare quasi-ductile PEF conveniently. First, we achieved this goal by optimizing the concentration of PMDA and the synthetic conditions of the polymer. On this basis, a series of PEF/TiO_2 nanocomposites with TiO_2 NPs (60 nm, 0.5-10‰ wt./wt. of PEF) were prepared; subsequently, the concentration that produced comprehensive excellent mechanical properties was selected, and PEF/nanocomposites with the addition of TiO_2 NPs (30 nm or 100 nm, 3‰) were also prepared as a contrast. The PEF/TiO_2 nanocomposites were characterized by ^1H NMR, FT-IR, XRD and SEM. The isothermal crystallization behavior, thermal and mechanical properties were investigated with DSC, TGA, and tensile testing. The barrier properties, anti-ultraviolet, anti-blue-

light and antibacterial functions were also assessed. Finally, the migration of TiO_2 from the polymeric matrix into different food simulants was evaluated for comparison with FDA and EU guidance to explain the biosafety of the material in food and cosmetics packaging field. PEF/TiO_2 nanocomposites were prepared by one-pot polycondensation method with chain extender and nano-TiO_2 in situ doping simultaneously, which provided a new idea for the modification of PEF.

2. Experimental

2.1. Experimental materials

Dimethyl 2,5-furandicarboxylate (DMFD, 98%) was obtained from Mianyang ChemTarget. Co. Ltd. (China). Ethylene glycol (EG, 99.8%), tetrabutyltitanate (TBT, 99%) and 1,1,2,2-tetrachloroethane (TCE, 98%) were purchased from Aldrich Co. Pyromellitic dianhydride (PMDA, 99%) used as chain extender and Titanium dioxide nanoparticles (TiO_2 NPs, primary particle size was 30 nm, 60 nm, 100 nm respectively, 99%) were purchased from Innochem. Phenol was purchased from Guangdong Guanghua Sci-Tech Co. Ltd. E. coli lyophilized powder was purchased from the mall North Na Chuanglian Biotechnology Co. LTD.

2.2. Synthesis of PEF_5 and PEF/TiO_2 nanocomposites

PEF/TiO_2 nanocomposites were also prepared using the one-pot polycondensation method (Fig. 1). The amounts of 60 nm-TiO_2 NPs were 0.5-10‰ (wt./wt. of the PEF). Among them, the concentration of TiO_2 NPs that produced the comprehensive mechanical properties was selected, and PEF/TiO_2 nanocomposites were prepared by adding 30 nm or 100 nm TiO_2 NPs (3‰). In order to obtain a uniform dispersion, TiO_2 NPs were added into the three-necked round-bottomed flask already filled with EG. Stirred it magnetically overnight with tinfoil wrapped to get the dispersion (Zhou et al., 2021)). After that, PMDA (5‰ mol/mol of DMFD), DMFD (DMFD: EG = 1:1.6, mol/mol) and TBT (2‰ mol/mol of DMFD) were successively added to the reactor according to the above method. The process of selecting PMDA content and polyester synthesis conditions could be found in the supplementary information. The sample named $PEF_{5,60,3}$ represented the nanocomposite materials with 5‰ concentration of PMDA and concentration of 60 nm-TiO_2 NPs (3‰) added in situ during the synthesis process. All the obtained polyesters were prepared as film materials according tosupplementary information (1.2).

2.3. Characterization

Nuclear Magnetic Resonance Spectroscopy (^{1}H NMR) measurement was carried out on a Bruker Avance 400-MHz spectrometer. PEF/TiO_2 nanocomposites were dissolved in trifluoroacetic acid-d (TFA) with tetramethylsilane (TMS) as the internal reference.

Weight-average molecular weight (M_w), number-average molecular weight (M_n) and its distribution (PDI) were determined by gel permeation chromatography (GPC) using a Waters 1515 HPLC apparatus. Hexafluorisopropanol (HFIP) supplemented with 0.005 mol/L sodium trifluoroacetate (CF_3COONa) was used as solvent at 30 °C and the solvent flow rate was 1.0 mL/min. M_w, M_n and PDI were determined using polymethyl methacrylate (PMMA) standard with a narrow PDI.

The η_{sp}/C were measured at 25 °C using an Ubbelohde viscometer (φ = 0.84). 0.125 g products were put into a 25 mL volumetric flask and dissolve by a mixture solvent composed of phenol and 1,1,2,2-tetrachloroethane (1/1, wt./wt.).

Fourier Transform Infrared Spectroscopy (FT-IR) was performed with a Shimadzu IRTracer-100 using a KBr pellet. In the absorbance mode, scans were collected in the spectral region of 400–4000 cm^{-1}.

The X-ray diffraction (XRD) patterns of polyesters were recorded using Empyream wide-angle X-ray scattering measurements and scanning speed of 12.5°/min over a range of 2θ = 5° to 80° at room temperature.

N_2 adsorption desorption tests were conducted on the prepared 30 nm, 60 nm, and 100 nm TiO_2 NPs using Quadrasorb evo N_2 adsorption–desorption.

The morphology of the PEF/TiO_2 nanocomposites after platinum coating was observed using scanning electron microscopy (SEM, Hitachi JSM-7800F) operated at an accelerating voltage of 3 kV.

Thermal transition properties and crystallization kinetics were performed by means of a Differential Scanning Calorimetry (DSC) on a DSC-25 thermal analyzer (TA Instrument, USA), calibrated with pure Indium and Zinc standards. Nitrogen gas flow rate was 50 mL/min. The samples were firstly heated from room temperature to 235 °C, and kept for 3 min to erase the thermal history, then cooled down to −20 °C, and then heated again to 235 °C, all rates were 10 °C/min. The total percentage crystallinity (X_c) of the sample was calculated by Eq. (1)

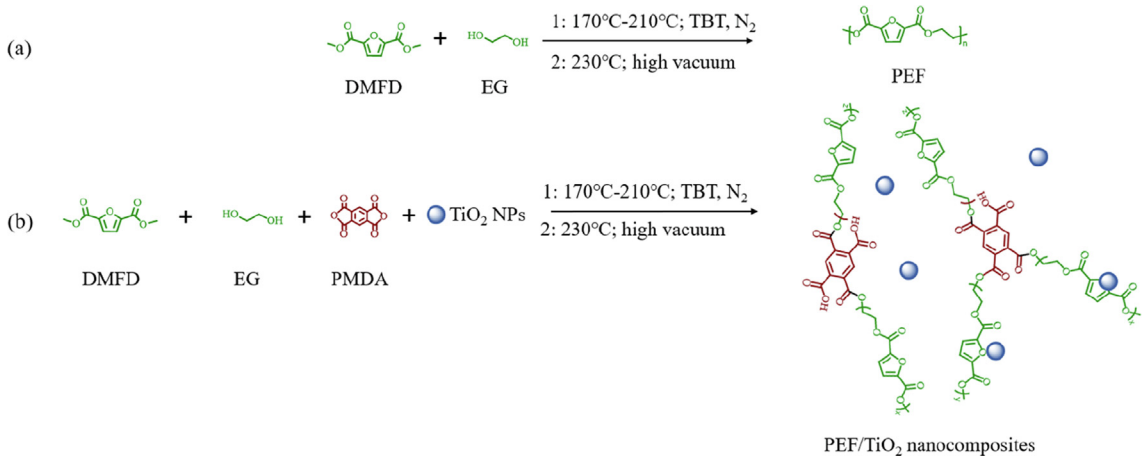

Fig. 1. Synthesis route of a) PEF was synthesized by transesterification fusion polycondensation b) PEF/TiO_2 nanocomposites was synthesized by the one-pot polycondensation.

$$X_c = \frac{\Delta H_m - \Delta H_{cc}}{\Delta H_m^0} \quad (1)$$

$\Delta H_m^0 = 140 Jmol^{-1}$ for 100% crystalline PEF (Qu et al., 2021)).

The characterization procedure of isothermal crystallization kinetics was set as follows: the samples were heated from the room temperature to 235 °C at the rate of 50 °C /min and kept for 3 min to eliminate the thermal history, then quenched directly to T_c and maintained at this temperature for melt crystallization. Cooling to −20 °C and maintained 1 min at the rate of 50 °C / min. Finally, they were raised to 235 °C at the rate of 10 °C /min. Crystallization temperatures T_c were varied from 145 °C to 175 °C. The relative crystallinity X_t can be calculated as Eq. (2):

$$X_t = \frac{\int_{T_0}^{T} \left(\frac{dH_c}{dT}\right) dT}{\int_{T_0}^{T\infty} \left(\frac{dH_c}{dT}\right) dT} \quad (2)$$

T_o, T, and T_∞ are the initial, arbitrary, and final crystallization temperatures, respectively.

TGA analysis was carried out using TGA-55 (TA Instrument, USA). About 5–10 mg samples were heating to 800 °C at a heating rate of 10 °C/min in a 50 mL/min flow of N_2.

Tensile modulus (Et), tensile strength (σ_m) and elongation at break (ε_b) of films were measured using a Instron 3366 with a strain rate of 0.5 mm/min at room temperature. The film samples were cut into rectangles strips (5 cm × 1 cm) and equilibrated under 50 ± 1% RH at 25 °C for 48 h. Film thickness was from the average of ten point determined by a digital micrometer with an accuracy of 0.01 mm. The impact strength was obtained from a film pendulum impact tester (FIT-01) produced by Labthink. Referring to the ASTM D3420 and GB 8809–88, the sample (ø=100 mm, thickness of 0.2 mm) was struck by the pendulum which impact energy was 1 J to evaluate its impact strength.

The CO_2 and O_2 barrier properties of the samples were investigated at 23 °C with the relative humidity (RH) of 50% by Labthink VAC-V2 gas permeability tester (0.1 Mpa), called manometric method. The CO_2 and O_2 used in the test process was 99.99%. The diameter of the film is 5 cm and thickness was from the average of ten point determined by a digital micrometer. Chamber and sample temperatures were controlled by an external thermostat. All experiments were run in triplicate.

The UV-shielding properties were measured by a Shimadzu (UV-2600) in the range of 200–800 nm. The UV blocking efficiency of the films was calculated according to the following Eq. (3):

$$\text{UVblocking}(\%) = 100 - \frac{\int_a^b T(\lambda) d\lambda}{\int_a^b d\lambda}\% \quad (3)$$

The antibacterial analysis of PEF_5 and PEF/TiO_2 nanocomposite films against the bacteria was studied. Gram-positive bacteria Escherichia coli (E. coli). Freeze-dried E. coli powder was transferred to sterilized solid medium for three consecutive days under aseptic conditions to obtain stably growing strains. Scrape 1 ∼ 2 scoops of single colony into sterilized tubes filled with liquid culture medium to get bacterial suspension, diluted into 10^5 CFU/mL of E. coli. Each test film (2 × 2 cm^2) was placed in sterilized petri dishes under aseptic conditions. 0.2 mL of bacteria suspension was added onto the surface of each film covered with sterilized polyethylene film. They were exposed to UV light (365 nm) illuminated by two 15 W black light lamps for 30 min (the samples were placed approximately 15 cm far from the lamps), and then incubated for 24 h at 37 °C. Then the samples and covering were washed with 20 mL 0.85% NaCl solution in order to remove the adhered bacteria. Quantification of colony review in eluate by aerobic plate count method and the antibacterial activity (R) was calculated by the following Eq. (4).

$$R(\%) = \frac{B - C}{B} \times 100 \quad (4)$$

where B is the average number of bacteria recovered from blank control samples, C is the average number of bacteria recovered from testing films.

The TiO_2 NPs migration test was conducted at room temperature (23 ± 2 °C). According to the recommendation from FDA and EU (European Union), distilled water, acetic acid, ethanol, and n-hexane were selected for the migration fluid, as neutral, acidic, alcohol and fat content, respectively. Each circular film sample (r = 2.5 cm, 0.5 g) was put into a 50 mL glass vial filled with 40 mL simulates, the whole film was immersed in the liquid, and the magnetic rotor was stirred in the bottle. The vial was kept at room temperature for 35 days. Remove 1 mL of solution every seven days, shaking each bottle by hand for half a minute before sampling to ensure uniform sampling. Digestion test of migration TiO_2 was based on Lian et al. and some modifications were made (Lian et al., 2016).) In brief, the 1 mL food simulant was placed in a pressure resistant glass container and 5 g of ammoniumsulfate ($(NH_4)_2SO_4$) and 10 mL of concentrated sulfuric acid (H_2SO_4, 98%) were incorporated. Those blend solutions were digested using oil bath at 200 °C for 3 h. After cooling at room temperature, the volume was fixed and tested by an inductively coupled plasma mass spectrometer (ICP-MS).

3. Results and discussion

3.1. Preparation of PEF and the extended PEF

PEF and the extended PEF were synthesized by one-pot polycondensation (transesterification and polycondensation). The gel content and η_{sp}/C of polyesters were determined, as shown in Table 1. The optimization process was described in detail in the supplementary information (1.2). After optimization of the PMDA content and synthesis conditions, the η_{sp}/C of polyester (PEF_5) was increased to 0.88 dL/g, and there was no gel content (less than 40%), which showed an improvement in the molecular weight of polyester.

The rheological characterization of PEF and the extended PEF was performed at 230 °C in Fig.S1. For Groups A and B, G', G" and η^* were proportional to the concentration of PMDA, polycondensation temperature and polycondensation time. The results showed that the viscoelasticity of polyester was improved by increasing the content of chain extender and optimizing the reaction conditions, showing the effectiveness of chain extension. In addition, the shear-thinning phenomenon was observed in all materials, in which η^* decreased as the angular frequency increased. This indicated that entanglement couplings occurred between the high molecular weight part and the part associated with the branches of the long branched chain, and a long time relaxation mechanism was thus generated (Pandey et al., 2020). Therefore, in addition to the highest η_{sp}/C, PEF_5 (obtained by condensation polymerization at 230 °C for 5 h) had the highest G', G" and η^*, which confirmed that polyester was chain-extended successfully. The Cole-Cole plot in Fig. S2 also confirmed that the chain extended products were significantly different from the pure PEF; the circular mark of the line type disappeared and the tails of the curve were upturned, confirming the existence of chain expansion.

3.2. Structure characterization

The structure of the prepared PEF_5 and PEF/TiO_2 nanocomposites was verified with FT-IR spectroscopy in Fig. 2a and Fig. S4. The peaks observed at 3128 cm^{-1}, 1581 cm^{-1}, and 1020 cm^{-1} corresponded to C–H, C = C, and C-O-C, respectively. The band peaking

Table 1
Gel content and η_{sp} /C of PEF and extended PEF.

Samples	PMDA content (‰)	Polycondensation condition	Gel content (%)	η_{sp}/C (dL/g)
PEF	0	230 °C × 4 h	2.5	0.20
$PEF_{0.5}$	0.5	230 °C × 4 h	2.4	0.27
PEF_1	1	230 °C × 4 h	2.8	0.39
PEF_3	3	230 °C × 4 h	3.5	0.65
PEF_5	5	230 °C × 4 h	4.7	0.73
PEF_7	7	230 °C × 4 h	56.7	–
PEF_5	5	240 °C × 4 h	45.3	–
PEF_5	5	250 °C × 4 h	72.8	–
PEF_5	5	230 °C × 5 h	5.5	0.88
PEF_5	5	230 °C × 6 h	41.3	–
PEF_5	5	230 °C × 8 h	85.5	–

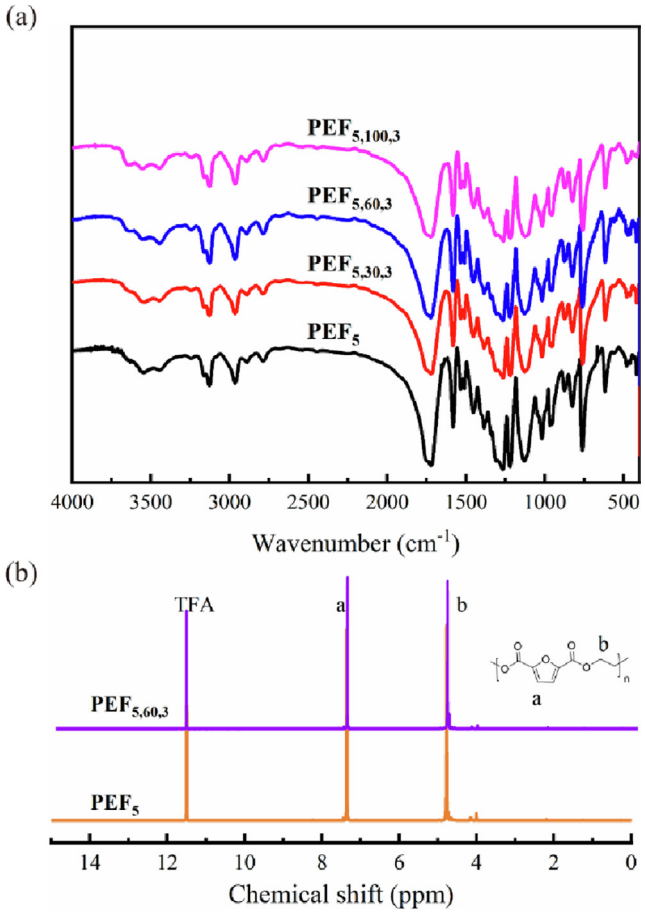

Fig. 2. FT-IR spectra a) and ^{1}H NMR spectra b) of PEF_5 and $PEF_{5,60,3}$.

at 2966 cm^{-1} was due to $-CH_2-$, and the peak at 1727 cm^{-1} corresponded to the C = O bond. The peaks at 958 cm^{-1}, 820 cm^{-1}, and 760 cm^{-1} were assigned to furan ring bending vibrations. The successful synthesis of PEF was confirmed by FT-IR results (Xie et al., 2020). Moreover, almost no difference was observed at the peak position, which suggested that the TiO_2 NPs and PEF_5 were physically doped without forming new bonds.

The chemical structures and compositions of PEF_5 and PEF/TiO_2 nanocomposites were characterized by ^{1}H NMR. Take PEF_5 and $PEF_{5,60,3}$, for example, shown in Fig. 2b. The protons attached to the furan ring showed chemical shifts at 7.36 ppm, and the protons of the glycol subunit appeared at 4.78 ppm. The area ratio of the two peaks was 1:2. The peak position was in accordance with the results reported in the literature (Achilias et al., 2017, Lotti et al., 2016), showing the successful synthesis of polyester. In addition, the branched structure of PEF was not shown in the FT-IR spectra and ^{1}H NMR spectra due to the low concentration of chain extender.

The sample named $PEF_{5,60,3}$ represented the nanocomposite materials with 5‰ concentration of PMDA and 3‰ concentration of 60 nm-TiO_2 NPs added in situ during the synthesis process. The η_{sp}/C of the PEF_5 and PEF/TiO_2 nanocomposites were 0.73-0.91 dL/g in Table 2, suggesting that high molecular weight nanocomposites had been synthesized successfully. The η_{sp}/C of PEF/nanocomposites increased with the TiO_2 nanoparticle feeding ratio up to 5‰, indicating that the presence of TiO_2 NPs contributed to the molecular weight growth of the polyester (Zhou et al., 2021). In addition, the M_n of PEF_5 and PEF/TiO_2 nanocomposites was higher than that of PEF (2.16 × 10^4 g/mol), which ranging from 3.12 × 10^4 g/mol to 5.48 × 10^4 g/mol. With the content of 60 nm TiO_2 particles increased, the M_n of the nanocomposite materials first increased and then decreased, reaching a maximum value of 5.48 × 10^4 g/mol at $PEF_{5,60,5}$. The nanocomposite materials with 30 nm or 100 nm TiO_2 NPs were also consistent with this rule, indicating that the content rather than the particle size of TiO_2 NPs had a greater effect on the molecular weight of polyester.

3.3. Morphology characterization

Fig. 3 shows the SEM micrograph to investigate the dispersion of TiO_2 NPs within the matrix materials as well as the fracture surface morphology of the films(Achilias et al., 2017). The PEF_5 in Fig. 3a showed smooth surface and compact structure with no particles. In sharp contrast, the PEF/TiO_2 nanocomposite films in Fig. 3-b-i presented much rougher surfaces and some crack tips, implying that the polymers exhibited ductile fracture and enhanced mechanical properties(Wu et al., 2019). In Fig. 3b-e, TiO_2 NPs presented fine dispersion inside the films as well as on the surface. However, some extent of agglomeration was found across the entire fracture surface at concentrations of 7‰ and above, and the size of TiO_2 NPs after agglomeration was still on the nanometer scale. In Fig. 3d and h-i, the higher the particle size of TiO_2, the more likely it was to aggregate. Almost no particle pull-out holes were observed in all pictures which also revealed that the interfacial adhesion between the matrix and TiO_2 particles used was strong (Can and Kaynak, 2019).

3.4. XRD characterization

Fig. 4 shows the XRD patterns of PEF_5 and PEF/TiO_2 nanocomposites. A broad peak appeared at 2θ of approximately 20° in each sample, proving that PEF_5 and PEF/TiO_2 nanocomposites were amorphous. The characteristic peak of anatase type TiO_2 appeared when the addition level reached 3‰ and above. The peaks at 2θ = 25.3°, 37.9°, 47.8°, 54.5°, 63.1°, 69.4° and 75.2° indicated that the

Table 2
The number average molecular weight (M_n), weight average molecular weight (M_w) and dispersity index (*PDI*) of PEF, PEF_5 and PEF/TiO_2 nanocomposites.

Samples	$M_n \times 10^4$ (g/mol)	$M_w \times 10^4$ (g/mol)	*PDI*	η_{sp}/C (dL/g)
PEF	2.16	3.18	1.47	0.20
PEF_5	3.90	10.38	2.66	0.81
$PEF_{5,60,0.5}$	4.08	9.77	2.39	0.77
$PEF_{5,60,1}$	3.92	13.87	3.54	0.73
$PEF_{5,60,3}$	4.23	15.52	3.67	0.89
$PEF_{5,60,5}$	5.48	17.43	3.18	0.91
$PEF_{5,60,7}$	3.24	15.12	4.67	0.87
$PEF_{5,60,10}$	3.12	10.04	3.22	0.81
$PEF_{5,30,3}$	4.95	12.63	2.55	0.90
$PEF_{5,100,3}$	4.22	9.93	2.35	0.83

crystal form of TiO_2 NPs had not been disturbed during the process. In addition, the intensity of the peaks and content of TiO_2 NPs were closely related, and the peaks of $PEF_{5,30,3}$, $PEF_{5,60,3}$ and $PEF_{5,100,3}$ were similar. The results were the same as those reported in the literature(Loos et al., 2020).

3.5. Crystallization behaviors

3.5.1. Non-isothermal crystallization

Fig. 5a-b and Table 3 depict the DSC thermograms records and results of PEF, PEF_5 and PEF/TiO_2 nanocomposites. The glass transition temperature (T_g) of PEF_5 was 1.8 °C higher than that of PEF (86.5 °C), while the melting point (T_m) was 8.8 °C lower than that of PEF. PEF exhibited a melting peak (ΔH_m = 33.8 J/g) at 216.8 °C in the second heating, higher than that of PEF_5 (15.9 J/g) at 208 °C. At the same time, there did not result in a noticeable change in T_g (approximately 88 °C) and T_m (approximately 208 °C) during the composite materials with different concentrations of 60 nm TiO_2 NPs, which possibly due to the relatively low concentration of TiO_2 NPs in composites (Luo et al., 2009). Until the addition amount reaches 8%, TiO_2 NPs showed an effect on the cold crystallization temperature of the substrate PLA (Luo et al., 2009). However, the T_m of $PEF_{5,30,3}$ and $PEF_{5,100,3}$ almost disappeared, which showed that the crystallization property was decreased, and the T_g was 1.3 °C-3.4 °C lower than that of $PEF_{5,60,3}$. It was reported that enthalpy relaxation peaks were observed, resulting in a T_g shift

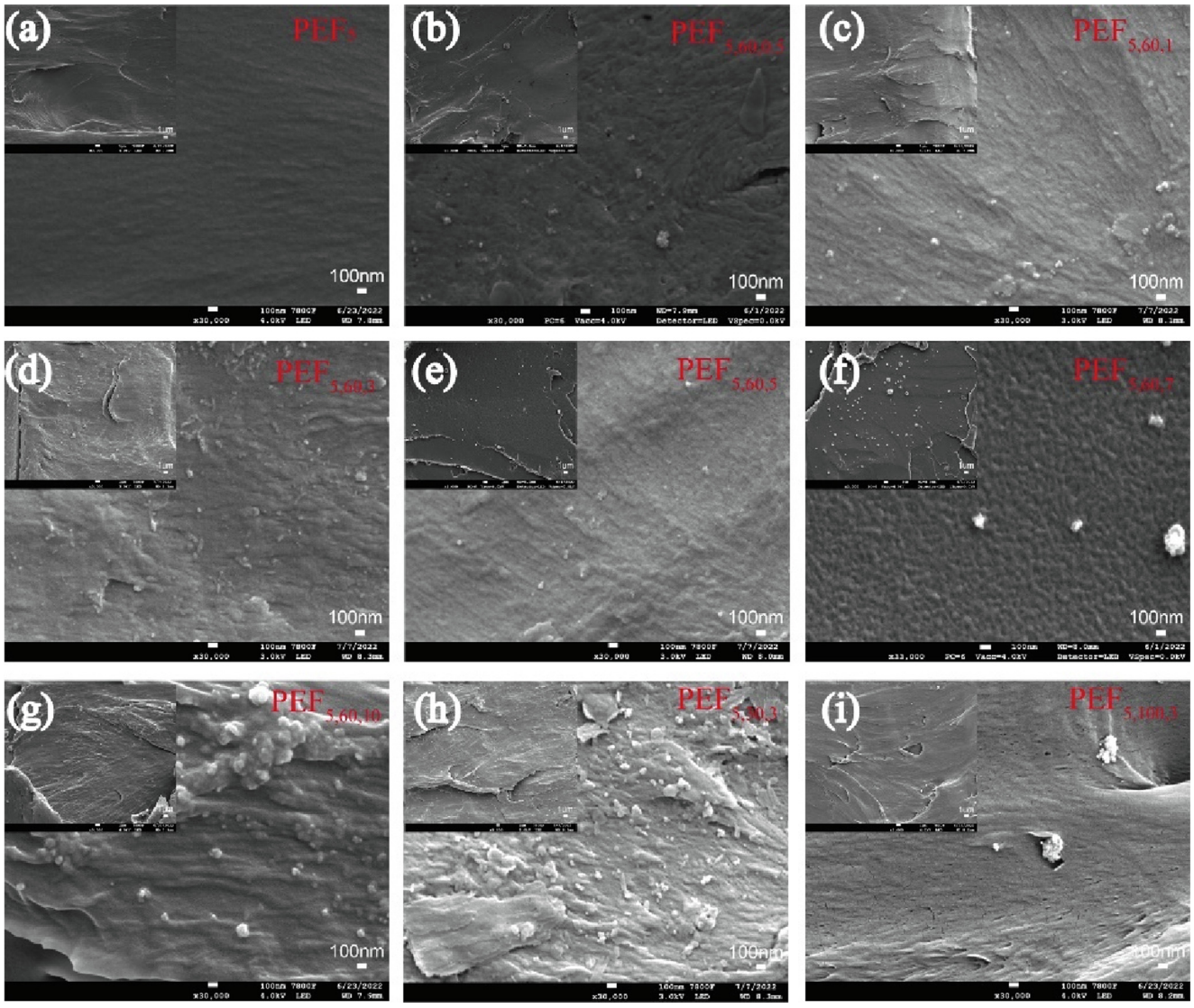

Fig. 3. SEM micrographs of the fractured surfaces of PEF_5 and PEF/TiO_2 nanocomposites: a) PEF_5, b) $PEF_{5,60,0.5}$, c) $PEF_{5,60,1}$, d) $PEF_{5,60,3}$, e) $PEF_{5,60,5}$, f) $PEF_{5,60,7}$, g) $PEF_{5,60,10}$, h) $PEF_{5,30,3}$, i) $PEF_{5,100,3}$.

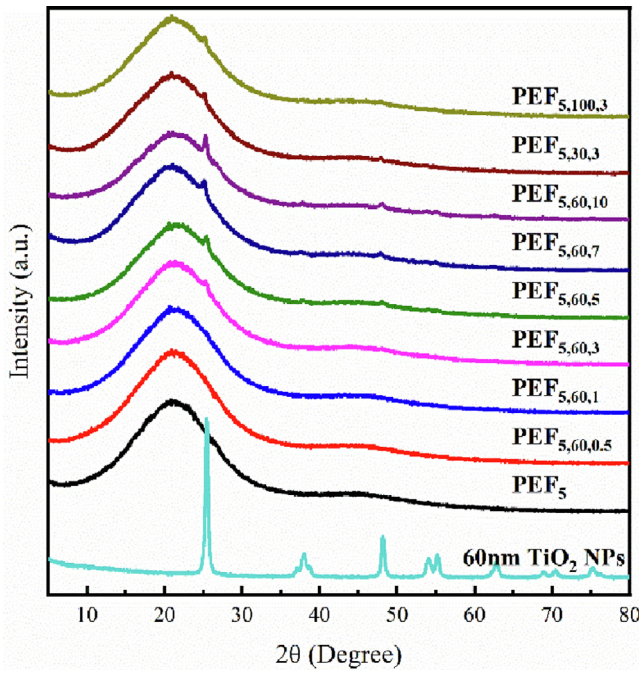

Fig. 4. XRD of PEF_5 and PEF/TiO_2 nanocomposites.

to a slightly higher temperature (Papageorgiou et al., 2022), agreeing with the phenomenon in this study.

Among all samples, the T_{cc} of PEF_5 and the nanocomposite materials (60 nm) was more obvious, probably due to the positive effect of chain extender on polyester crystallization and the nucleating agent effect of 60 nm TiO_2. The accelerated crystallization rate of polyester might be attributed to the nucleation effect when TiO_2 NPs were uniformly distributed, but at high concentrations, nanoparticles might agglomerate to prevent the formation of nucleation sites and hinder the continuous growth of crystals (Vassiliou et al., 2008, Tang et al., 2016).

3.5.2. Isothermal crystallization

The isothermal crystallization properties of the PEF_5 and PEF/TiO_2 nanocomposites (60 nm) were also investigated by DSC. Fig. 6a and Fig. S7 depicted the thermograms recorded during successive heating for samples crystallized from the melt at different isothermal crystallization temperatures (T_c) ranging from 140 °C to 175 °C. All samples showed wide crystallization peaks, and the curves at each sample shifted with the isothermal temperature. To quantitatively study the crystallinity behavior, the relative crystallinity (Xt) and semi-crystallization time ($t_{1/2}$) at different temperatures were calculated. The Xt versus time and $t_{1/2}$ versus temperature curves are shown in Fig. 5a-b and Fig. S8. The $t_{1/2}$ showed a trend of decreasing and then increasing in the range of 145 °C-175 °C, and reached the lowest at 160 °C (Stoclet et al., 2015). The $t_{1/2}$ of all samples ranged from 5.7 min to 9.66 min at 160 °C and reached the fastest at $PEF_{5,60,3}$ of only 6.16 min, which was increased by 21.8% compared with PEF_5 (except for 5.7 min at $PEF_{5,60,1}$, which was attributed to the low molecular weight). It was reasonable that the variation pattern remained consistent with T_{cc} in Fig. 6d. Inorganic nanoparticles primarily have two effects on the crystallization of materials in nanocomposites: One is the reduction in chain segment mobility, and the other is the contribution of nanoparticles to heterogeneous nucleation (Nikam and Deshpande, 2019, Farhoodi et al., 2013). These heterogeneous nucleation sites could adsorb polymer chains in the melt for orderly arrangement to form crystal nucleus (Kourtidou et al., 2023) Hao et al.'s research showed that TiO_2 NPs impart the smaller and more defects spherulites to the resulting nanocomposites, resulting in a decrease in T_m of the nanocomposite materials, which is consistent with the results of this article (Li, 2006).

In short, the crystallization rate was related to the isothermal crystallization temperature, concentration and dispersion of nanoparticles in the matrix (Luyt and Gasmi, 2017, Nikam and Deshpande, 2019). Moreover, the $t_{1/2}$ values of PEF_5 and PEF/TiO_2 nanocomposites were much lower than the 18.2 min-40.3 min reported in the literature, which their molecular weight ranged from 12000 g/mol to 28000 g/mol (Stoclet et al., 2015, van Berkel et al., 2015).

3.6. Thermal stability

The thermal stability of the PEF, PEF_5 and PEF/TiO_2 nanocomposites was determined by TGA, as shown in Fig. 5c-d and Table 4. PEF and PEF_5 presented similar $T_{d,5\%}$ and T_{dmax} of 369 °C and 14%, respectively. The $T_{d,5\%}$ and T_{dmax} increased with increasing concentration of 60 nm TiO_2, and they were approximately 2.1 °C-4.4 °C and 2.8 °C-11 °C higher than those of PEF_5 at 369.9 °C and 409.7 °C, respectively. Naturally, as the concentration of inorganic particles increased, so did the residual amount. This could be attributed to the assumption of physical interactions between TiO_2 NPs and the matrix, which required higher thermal energy to disrupt these interactions, thereby improving the thermal stability of nanocomposites (Youssef, Abd El-Aziz and Morsi, 2022). $PEF_{5,30,3}$ and $PEF_{5,100,3}$ had higher $T_{d,5\%}$ and T_{dmax} than $PEF_{5,60,3}$, showing the different thermal properties of PEF/TiO_2 nanocomposites with different particle sizes. In the substrate material, TiO_2 NPs could play a physical crosslinking role to improve the thermal stability of polyester (Vassiliou et al., 2008). The excellent thermal stability was of great importance for determining their potential application.

3.7. Mechanical properties

The film of pure PEF was brittle and have not been tested for tensile strength. The PEF_5 and PEF/TiO_2 nanocomposites were subjected to tensile and impact experiments at room temperature, and the results are summarized in Table 5. The E_t of the PEF/TiO_2 nanocomposites was higher than that of PEF_5 (an increase of 9%∼16%), except for $PEF_{5,60,1}$ (due to its low molecular weight). With the increase in the content of 60 nm TiO_2 NPs, the E_t showed a trend of increasing from PEF_5 (2158 MPa) first and then decreasing to $PEF_{5,60,10}$ (2038 MPa). The improvement in the E_t of nanocomposites by the addition of stiff TiO_2 NPs was expected at low concentration, this was due to the stiff structure of TiO2 NPs and the close connection between the TiO_2 NPs and the matrix (shown in Fig. 3); however, high concentrations of TiO_2 nanoparticles might reduce the E_t of nanocomposites due to agglomeration (Gomez-Hermoso-de-Mendoza et al., 2020, Can and Kaynak, 2019). The ε_b of most nanocomposites was lower than that of PEF_5, which is also similar to that reported in the literature (Can and Kaynak, 2019). TiO_2 NPs fillers as heterogeneous solid nanoparticles may prevent polymer stress-induced crystallization, reducing the fracture resistance of the complex network, according to research by Farhodi et al. The decrease in fracture elongation of nanocomposites was consistent with this research's findings (Farhoodi et al., 2013). Compared with PEF_5, $PEF_{5,60,3}$ had the best comprehensive performance and its E_t, σ_m and ε_b increased by 36%, 14%, and 16%, respectively. However, the E_t of $PEF_{5,30,3}$ and $PEF_{5,100,3}$ was increased by only 2% and 10%, respectively, compared with PEF_5. The impact strength of PEF_5 showed a great improvement compared with PEF in this study (the film prepared by PEF was brittle), proving that the addition of chain extender was effective for the preparation of quasi-toughness polyester. The impact strength of

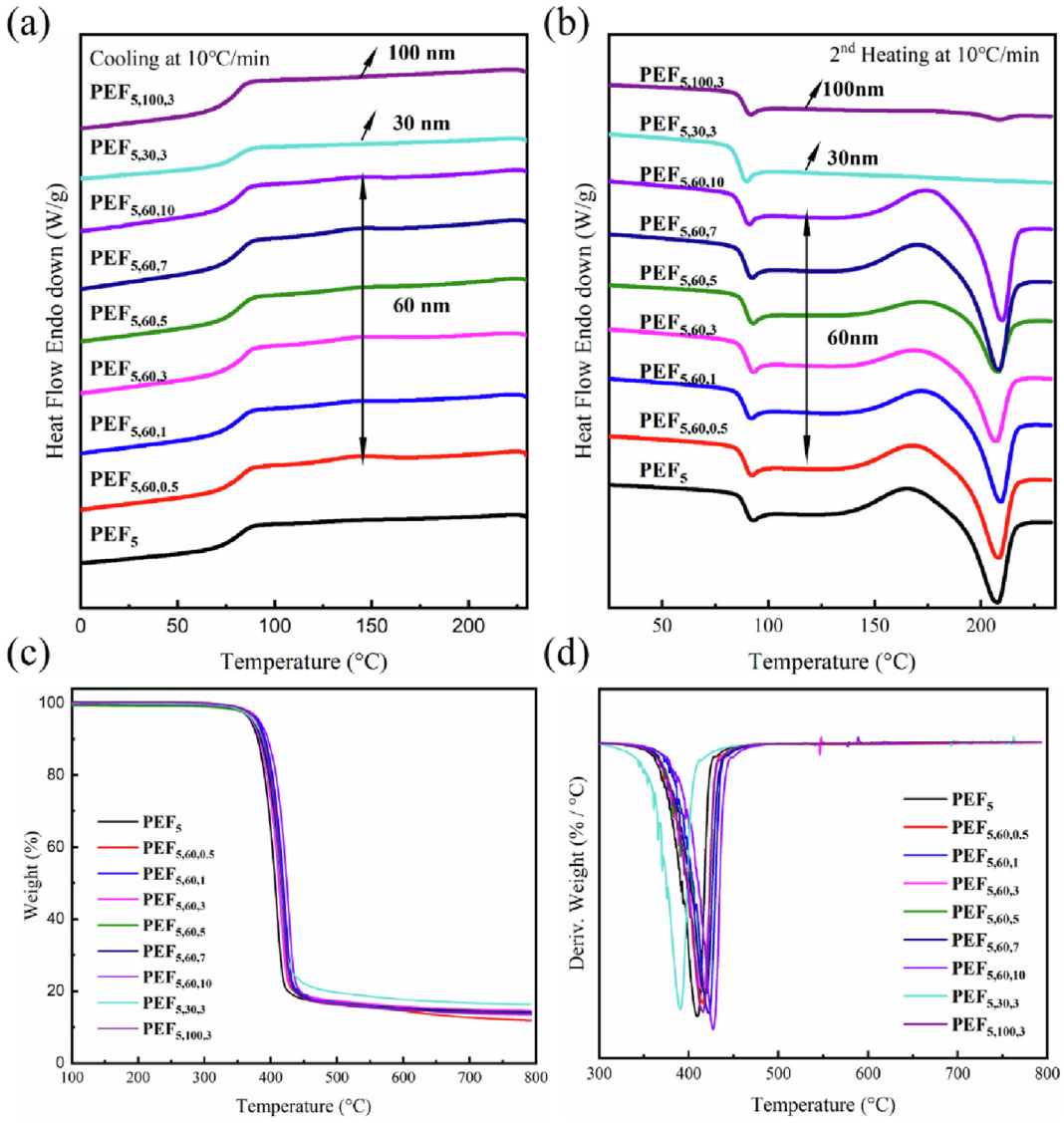

Fig. 5. DSC a, b) and TGA c, d) curves of PEF, PEF_5 and PEF/TiO_2 nanocomposites under N_2 atmosphere.

Table 3
Thermal properties data of PEF, PEF_5 and PEF/TiO_2 nanocomposites obtained by DSC.

Polymers	Cooling		2nd heating					
	T_c (°C)	ΔH_c (J/g)	T_g (°C)	T_{cc} (°C)	ΔH_{cc} (J/g)	T_m (°C)	ΔH_m (J/g)	X_c (%)
PEF	148.7	9.4	86.5	162.1	16.2	216.8	33.8	12.5
PEF_5	142.4	2.3	88.3	164.9	9.2	208.0	15.9	4.8
$PEF_{5,60,0.5}$	141.6	7.8	88.0	167.9	7.7	208.4	14.9	5.0
$PEF_{5,60,1}$	145.3	4.3	88.2	160.1	7.8	208.3	23.0	10.7
$PEF_{5,60,3}$	146.8	1.1	88.7	168.3	5.4	207.3	8.7	2.3
$PEF_{5,60,5}$	145.4	0.7	88.6	172.1	5.8	208.1	8.6	2.0
$PEF_{5,60,7}$	144.1	0.9	88.2	169.7	9.6	208.5	16.8	5.1
$PEF_{5,60,10}$	144.8	1.2	88.1	169.6	7.9	207.8	14.3	4.5
$PEF_{5,30,3}$	–	–	85.3	–	–	–	–	–
$PEF_{5,100,3}$	–	–	87.4	–	–	208.4	0.9	–

PEF_5 (2.04×10^3 J/m^2) was lower than that reported in the literature (7.2×10^3 J/m^2) (Zhang et al., 2020), which was significantly improved in nanocomposite materials. The impact strength of the PEF/TiO_2 nanocomposites showed a strict growth law from 10.4×10^3 J/m^2 to 52.5×10^3 J/m^2 with increasing of TiO_2 NPs concentration ($PEF_{5,30,3}$ and $PEF_{5,100,3}$ also included). This improvement in impact strength was also expected, which might be due to the ability of nanoparticles to fill holes or defects in the material, thus increasing the stress on the surface where the stress was evenly distributed (Zhang et al., 2021, Al-Zubaydi, Salih and Al-Dabbagh, 2020, Zhang et al., 2020). The tight connection between the matrix and the nanoparticles was more conducive to stress

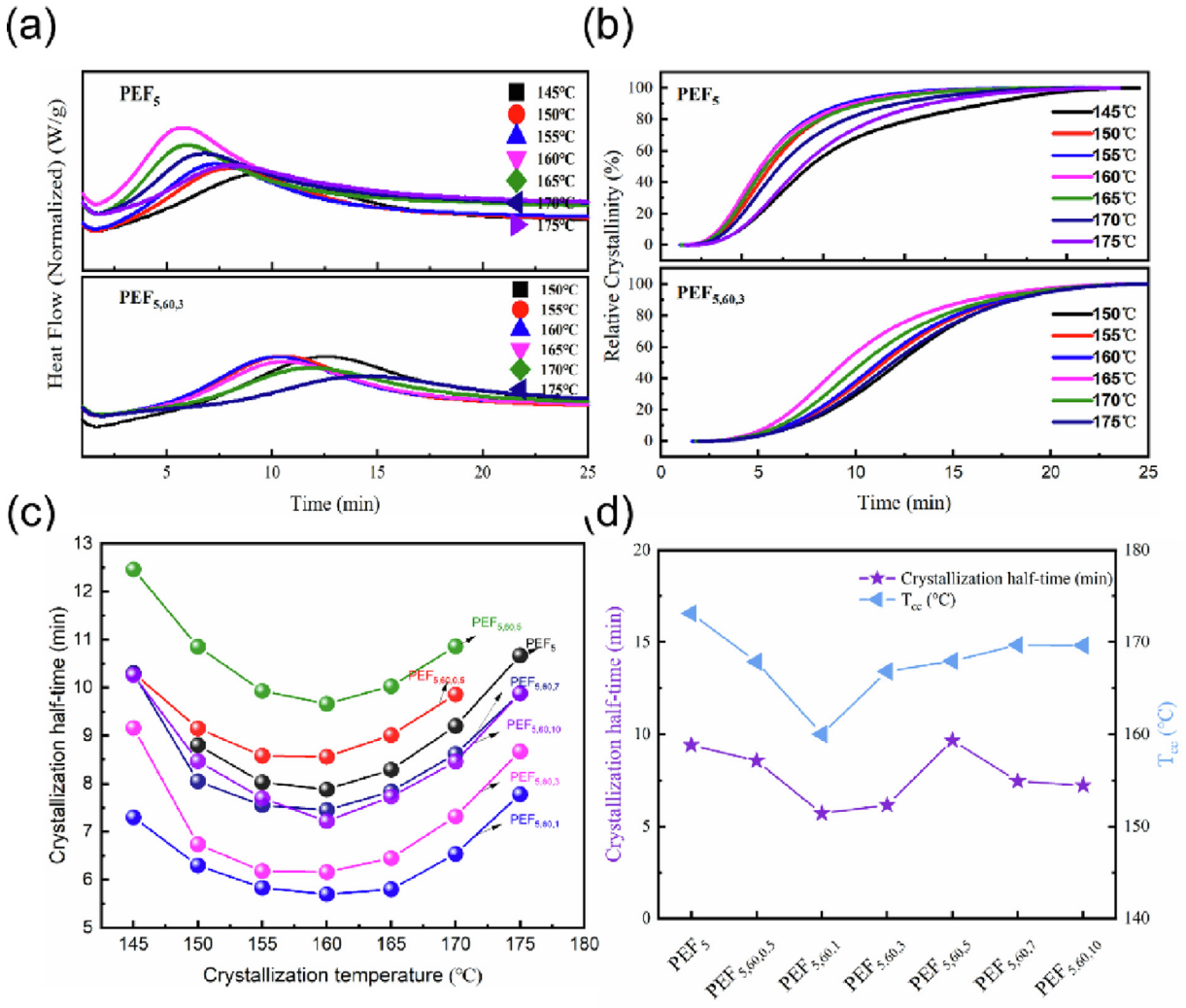

Fig. 6. Isothermal crystallization of PEF_5 and PEF/TiO_2 nanocomposites: a, b) DSC traces of isothermal crystallization of samples within 25 min, c) crystallization half-time of samples at various temperatures, d) crystallization half-time at 160 °C and cold crystallization temperature of samples.

Table 4
Thermal properties data of PEF, PEF_5 and PEF/TiO_2 nanocomposites obtained by TGA.

Polymers	$T_{d,5\%}$[a] (°C)	T_{dmax}[b] (°C)	R_{600}[c] (wt%)
PEF	369.4	416.1	14.0
PEF_5	369.9	409.7	14.9
$PEF_{5,60,0.5}$	373.9	415.8	14.5
$PEF_{5,60,1}$	372.6	412.5	15.3
$PEF_{5,60,3}$	372.0	415.5	15.7
$PEF_{5,60,5}$	373.7	418.9	15.3
$PEF_{5,60,7}$	374.3	418.5	15.2
$PEF_{5,60,10}$	374.0	420.7	15.1
$PEF_{5,30,3}$	375.0	417.1	17.6
$PEF_{5,100,3}$	378.8	420.0	14.7

[a] $T_{d,5\%}$ represents the initial degradation temperature at a mass loss of 5%.
[b] T_{dmax} represents the maximum mass loss temperature where maximum loss rate takes place.
[c] R_{600} represents the residual amount at 600 °C.

transfer, thereby delaying crack propagation (Can and Kaynak, 2019).

3.8. Barrier properties

The CO_2 and O_2 permeability of PEF_5 and PEF/TiO_2 nanocomposites were determined by the differential pressure method, and the effects of content and particle size were also discussed in Table 6. In this study, all materials presented higher barrier properties compared to PET and PLA materials, and the permeability of CO_2 was slightly higher than that reported in the literature. It was reported that large pores between molecules lead to higher gas and liquid permeability due to the formation of branched structure. The polymer prepared by PET and PMDA showed higher carbon loss (13.5% for PET and 15% for branched PET), which showed that the formation of a branched structure improved the permeability rate of CO_2 (Awaja and Pavel, 2005). The permeability of CO_2 increased with the addition of TiO_2 NPs, from 0.037 barrer for PEF_5 to 0.063 barrer for $PEF_{5,60,10}$; however, the barrier performance of O_2 became better, and the BIF value increased from 1.1 for PEF_5 to 2.6 for $PEF_{5,60,0.5}$. The most likely value of CO_2/O_2 in nanocomposite materials was located at $1 \sim 2$, higher than PEF_5, which was 0.67. Despite this, the CO_2 and O_2 barrier properties of the PEF/TiO_2 nanocomposites were still in the same order of magnitude and maintained excellent gas barrier properties. Similar to the findings reported by Silva-Leyton et al., the tendency of composite materials towards CO_2 and O_2 was not significant (Silva-Leyton et al., 2019). The good barrier performance of the composite material is unaffected by the TiO_2 NPs due to their small particle size, low concentration, and physical doping.

Table 5
Mechanical properties data obtained by stress–strain measurements.

Sample	E_t[a] (MPa)	σ_m [b] (MPa)	ε_b^c (%)	Impact strength ($\times 10^3$, J/m^2)
PEF_5	2158 ± 84[d]	67 ± 10	4.4 ± 0.1	2.04
$PEF_{5,60,0.5}$	2351 ± 183	82 ± 5	5.6 ± 1.1	10.4
$PEF_{5,60,1}$	2118 ± 184	63 ± 8	4.1 ± 1.0	19.5
$PEF_{5,60,3}$	2485 ± 78	74 ± 4	4.0 ± 0.2	21.3
$PEF_{5,60,5}$	2483 ± 14	49 ± 3	2.5 ± 0.2	28.7
$PEF_{5,60,7}$	2511 ± 77	60 ± 6	3.3 ± 0.5	50.6
$PEF_{5,60,10}$	2038 ± 19	47 ± 5	3.0 ± 0.3	52.2
$PEF_{5,30,3}$	2191 ± 194	71 ± 12	4.5 ± 1.7	18.3
$PEF_{5,100,3}$	2368 ± 68	58 ± 17	3.4 ± 1.4	19.0

[a] Et = Tensile modulus, [b]εb = elongation at break, [c]σ_m = maximum tensile stress, [d] "±" refers to the mean standard deviation.

Table 6
CO_2 and O_2 barrier properties of PEF_5 and PEF/TiO_2 nanocomposites.

Sample	CO_2 permeability coefficient (barrer[a])	BIF_p[b]	O_2 permeability coefficient (barrer)	BIF_p	CO_2/O_2
PET (Wang et al., 2016, Wang et al., 2017b)	0.13	1	0.060	1	2.17
PLA (Hu et al., 2019b)	1.0	0.13	0.25	0.24	4.00
PEF(Wang et al., 2017b)	0.010	13.0	0.011	5.5	0.9
PEF_5	0.037	3.5	0.055	1.1	0.67
$PEF_{5,60,0.5}$	0.043	3.0	0.023	2.6	1.87
$PEF_{5,60,1}$	0.076	1.7	0.048	1.3	1.58
$PEF_{5,60,3}$	0.043	3.0	0.044	1.4	0.98
$PEF_{5,60,5}$	0.059	2.2	0.057	1.1	1.04
$PEF_{5,60,7}$	0.043	3.0	0.041	1.5	1.05
$PEF_{5,60,10}$	0.063	2.1	0.054	1.1	1.17
$PEF_{5,30,3}$	0.045	2.9	0.034	1.8	1.35
$PEF_{5,100,3}$	0.059	2.2	0.066	0.9	0.89

[a] 1 barrer = 10^{-10} cm^3·cm/cm^2·s·cmHg, [b] Barrier Improvement Factor (BIF_P): the permeability coefficient of CO_2 or O_2 in PET divided by the CO_2 or O_2 permeability in other materials, the higher the BIF_P, the better the barrier.

3.9. Anti-ultraviolet and anti-blue-light functions

To examine the optical absorption study of 30 nm TiO_2 NPs, 60 nm TiO_2 NPs and 100 nm TiO_2 NPs by UV-vis, Diffuse reflectance (DRS) spectra and results are shown in Fig. 7a. All three curves demonstrated a cutoff absorption edge at approximately 410 nm, which exhibited a similar pattern to the unmodified TiO_2 NPs reported in the literature(Kite et al., 2021). This indicated that the change in particle size of TiO_2 NPs did not result in a difference in the bandgap of the sample. From Fig. 7b, it could be seen that the bandgap energy values of 30 nm, 60 nm, and 100 nm TiO_2 NPs were 2.90 eV, 2.84 eV, 2.77 eV, respectively. TiO_2 is an N-type semiconductor. When ultraviolet light with a wavelength less than 385 nm irradiates TiO_2, electrons in the valence band can absorb ultraviolet light and be excited to the conduction band, producing electron hole pairs. In this excited state, electrons generated by light can recombine with holes, during which light energy can be converted into heat or other forms of energy. Therefore, TiO_2 has the function of absorbing ultraviolet light(Zhou et al., 2021).

Photographs of the PEF_5 and PEF/TiO_2 nanocomposite films are shown in Fig. 8a. The PEF_5 film was colorless and transparent. With increasing of 60 nm-TiO_2 NPs concentration, the transmittance of the films decreased and showed a white color gradually to varying degrees. The ultraviolet–visible light spectra (200 nm to 800 nm) are shown in Fig. 8b, which shows that all the films had decreasing transmittance as the wavelength of light decreased. All films exhibited an obvious shielding effect on UVB (280 nm-320 nm) and UVC (220 nm-280 nm), and the blocking rate shown in Fig. 8c increased from 98.43% to 99.95% and from 99.92% to 99.96%, respectively. In the UVA (320 nm-400 nm) region, the decrease in transmittance indicated the effect of TiO_2 NPs on the anti-ultraviolet properties of films, and the blocking rate changed from 45.38% to 93.54%. The $PEF_{5,60,3}$ prevented 72.49% of UVA range, and the blocking rate of $PEF_{5,30,3}$ and $PEF_{5,100,3}$ was 76.80% and 76.53%, respectively, which showed excellent ultraviolet shielding properties with a very small amount of TiO_2 nanoparticles. The shielding effect of ultraviolet light could effectively reduce the deterioration of packaging contents, and extend the life of the film. The blocking rate of blue light (400 nm-500 nm) in different bands also increased with the increasing nanoparticle concentration, from 21.5% to 74.3% at 400 nm-450 nm, and from 16.7% to 64.9% at 450 nm-500 nm. Among them, high-frequency shortwave blue light (400 nm-450 nm) is more harmful to the human body, mainly causing retinal damage (Yang et al., 2020). PEF_5 showed a high degree of transparency, which was 89.2% at 800 nm, followed by a progressively decreasing value with increasing TiO_2 content. $PEF_{5,60,10}$ maintained the lowest transmittance, which was only 55.9% at 800 nm. These results indicated that the higher the concentration of TiO_2 NPs, the better anti-ultraviolet and anti-blue-light properties were obtained, although the transparency was reduced.

3.10. Antibacterial properties

TiO_2 NPs, Ag NPs, CuO NPs have demonstrated successful antimicrobial activity in food packaging materials(He et al., 2016, Kim et al., 2007, Siripatrawan and Kaewklin, 2018). The antibacterial properties of PEF_5 and PEF/TiO_2 nanocomposite films against the E. coli were studied in Fig. 9a (He et al., 2016). As expected, the PEF_5 film did not show significant antibacterial activity; however, nanocomposites with TiO_2 NPs exhibited strong antibacterial activity against gram-negative bacteria (E. coli) under UV light. With the increase in the amount of TiO_2 NPs added, their antibacterial rate against E. coli also gradually increased, from 2% of PEF_5 to 83% of $PEF_{5,60,10}$. TiO_2 NPs undergoes photocatalytic reactions when illuminated with UV light, generating electrons (e^-) and holes

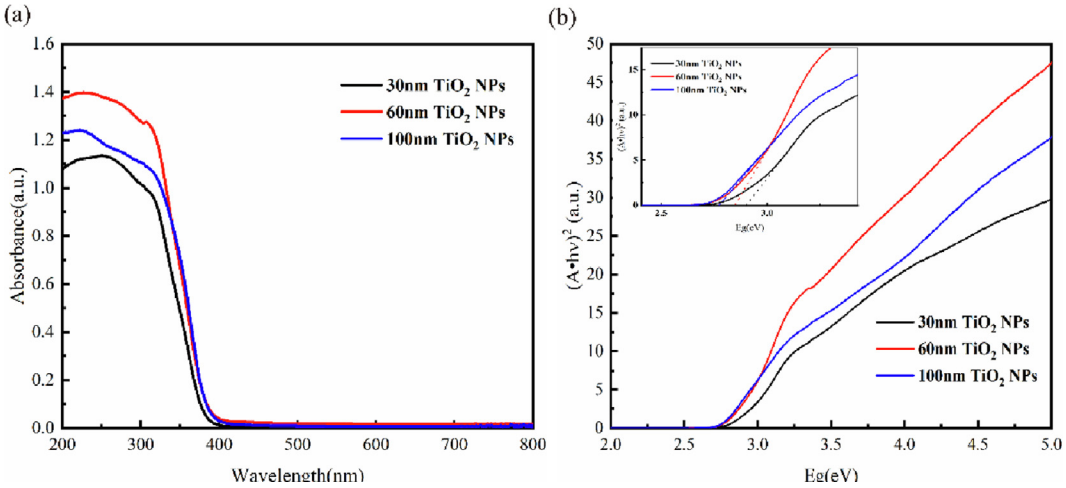

Fig. 7. a) uv-vis DRS spectra and b) Tauc's plots of TiO_2 NPs.

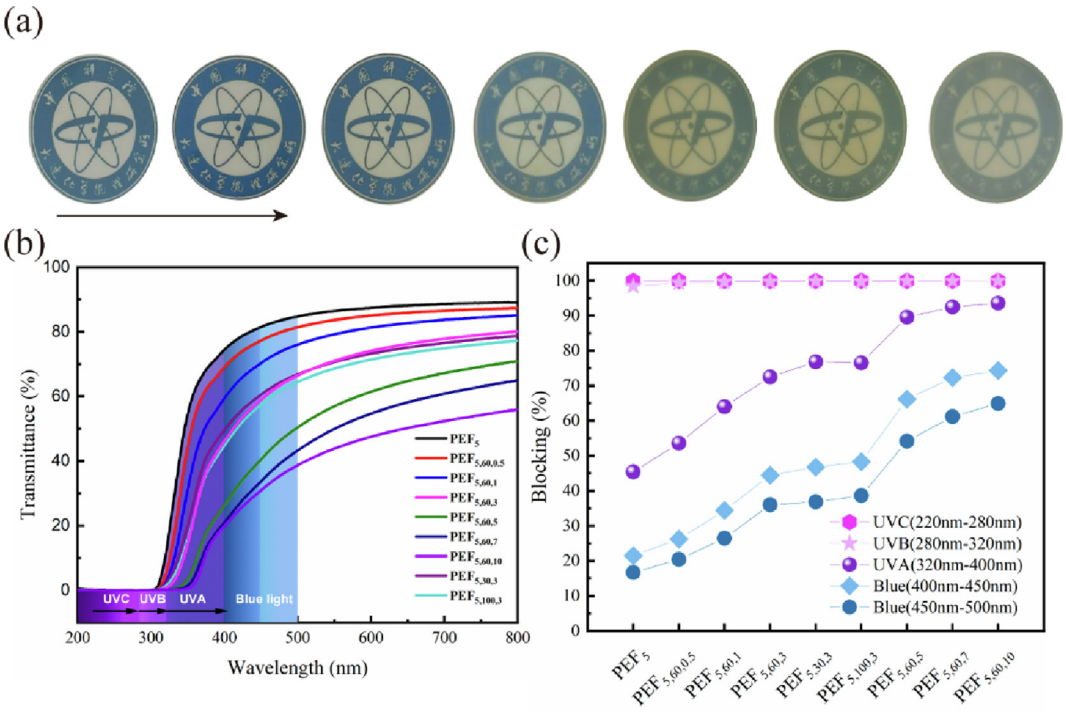

Fig. 8. a) digital photos, b) uv–vis spectra and c) uv blocking parameters of pef_5 and PEF/TiO_2 nanocomposites.

(h^+), which could react with substances in the air and generated O_2^- and OH•, respectively (Siripatrawan and Kaewklin, 2018, He et al., 2016, Zhang et al., 2022a). It was reported that ROS such as O_2^- and OH• could oxidize polyunsaturated phospholipids in microbial cell membranes, causing changes in cell morphology and cytoplasmic leakage to achieve sterilization purposes (Siripatrawan and Kaewklin, 2018). Therefore, when irradiated TiO_2 nanoparticles come into contact with microorganisms, these active substances easily cause cell lysis. The higher the TiO_2 content was, the more reactive oxygen species were generated, and the resultant antibacterial rate substantially increased.

3.11. Migration of titanium

A migration experiment was set up to study the safety of PEF_5 and PEF/TiO_2 nanocomposites used in the food or cosmetics packaging industry, where migration of nanoparticles would result in oral intake or dermal exposure. To the best of our knowledge, there were no specific guidelines concerning packaging/content interaction studies, but the migration behavior of polymer/nanocomposite materials used as cosmetic packaging was studied with reference to the standards of food contact materials (Connolly et al., 2019). The migration assay was set up to determine the rate of TiO_2 NPs migration to the simulated solution during 35 days of storage, as shown in Fig. 9b. According to the European Commission 2011 (Lian, Zhang and Zhao, 2016, Liu et al., 2016) and GB/T 23296.1, distilled water, 3% acetic acid, and ethanol were used to simulate aqueous, acidic, and alcoholic foods, while n-hexane was the fatty food simulant. For 3% acetic acid, the migration rates ranged from 0.50 to1.82 μg/g with increasing of TiO_2 NPs concentration within 35 days, which was far lower than the regulation given by the European Food Safety Authority (maximum migration

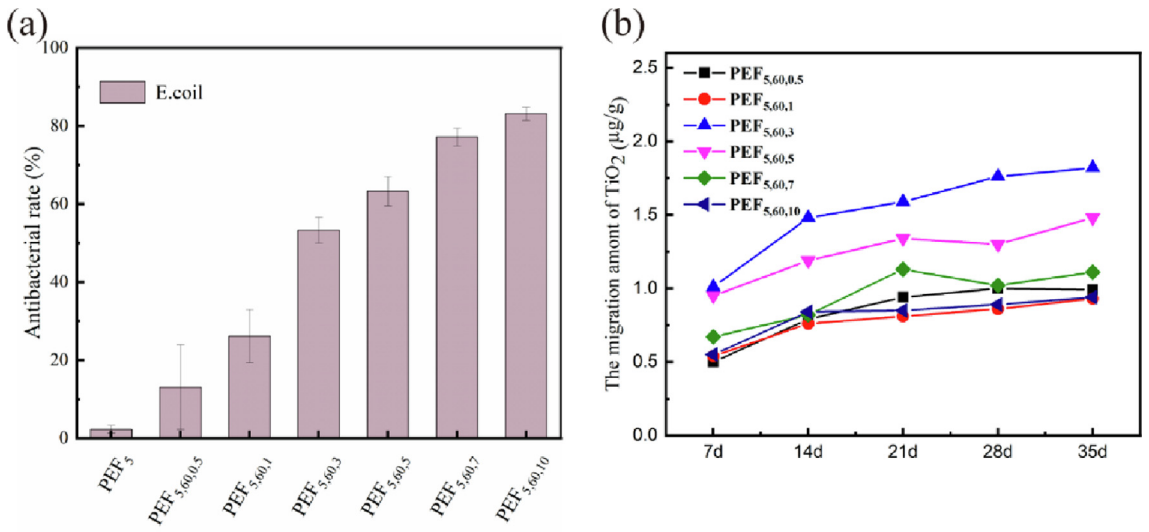

Fig. 9. a) growth inhibition of pef_5 and PEF/TiO_2 nanocomposites against E. coli, b) The migration amount of TiO_2 NPs in 3% acetic acid solution.

of TiO_2 particles in food packaging materials was 10 mg/kg) (Tang et al., 2020). The FDA approved the use of TiO_2 in foods as a color additive (E171) at levels up to 1% (Alizadeh-Sani, Mohammadian and McClements, 2020); however, titanium dioxide was only used as an additive in food contact plastics without specifying the migration amount but only the purity in GB 9685–2016. In addition, TiO_2 was also commonly used as a sunscreen, whitening agent, and oil absorber in cosmetics. The value of TiO_2 NPs in other simulated solutions was lower than the detection limit of the instrument, showing that the effect of the type of simulated solution on the migration of TiO_2 NPs in composite films was significant. The swelling of nanocomposite materials in acetic acid solution and the reduced barrier properties of the materials enhance the migration of nanoparticles. However, due to the solvent resistance of the PEF material, the barrier formed by the ethanol solution on the membrane surface will prevent the further migration of the nanoparticles (Li et al., 2016). Hence, acidic food was more conducive than other simulation solutions, such as ethanol, water, and hexane.

For each sample, the amount of migration in acetic acid solution increased with time, but the dependence of the rate on concentration was not obvious. Since TiO_2 NPs on the surface instead of the titanium inside the film of the PEF film would migrate to the solution, it could be seen that as the concentration of TiO_2 nanoparticles increased, there might be more nanoparticles on the membrane surface. The migration of titanium increased first and then decreased with increasing concentration of TiO_2 NPs, and a turning point occurred at $PEF_{5,60,3}$, which might be due to agglomeration at high concentrations, inlaid in the polyester internal network structure and not easily migrating out. The migration amount of $PEF_{5,60,1}$ became low (due to its low molecular weight results and higher crystallinity). The dispersion and agglomeration state of the nanoparticles were also demonstrated in Fig. 3. The results indicated that the migration of TiO_2 NPs from the nanocomposite packaging into simulated solution was below the EU and FDA recommended limits.

4. Conclusion

In summary, PEF/TiO_2 nanocomposites with excellent performance were successfully synthesized via one-pot polycondensation. The addition of 5‰ PMDA not only extended the chain of PEF but also enhanced its toughness. In these nanocomposites, TiO_2 NPs were physically incorporated into the polymer matrix with homogeneous dispersion below 5‰. All PEF/TiO_2 nanocomposites in the form of powder were amorphous. The T_gs with 60 nm TiO_2 NPs (~88 °C) were higher than that of pure PEF. However, nanocomposites with 30 nm and 100 nm TiO_2 presented relatively lower T_g. The $T_{d,5\%}$ and T_{dmax} of PEF/TiO_2 nanocomposites increased with increasing addition percentage. Only 60 nm TiO_2 could enhance the crystallization rate of nanocomposites. The crystallization rate increased first and then decreased with increasing TiO_2 content of 60 nm. The $t_{1/2}$ of $PEF_{5,60,3}$ reached a minimum (6.16 min) and was less than that of pure PEF (18.2 min-40.3 min) at 160 ℃. As the 60 nm TiO_2 content increased, the tensile modulus of the nanocomposites first increased and then decreased, and the impact strength increased. For $PEF_{5,60,10}$, its impact strength was 52.2 × 10^3 J/m^2, which was 25 times that of pure extended PEF (2.04 × 10^3 J/m^2). Fortunately, all PEF/TiO_2 nanocomposites maintained higher gas barrier properties than traditional packing materials. Meaningfully, due to the addition of TiO_2 NPs, nanocomposites were endowed with excellent anti-ultraviolet, anti-blue-light and antibacterial functions. The migration rate of TiO_2 NPs in water, ethanol, n-hexane and acetic acid solution was lower than the EU and FAD for standard packaging materials for food and cosmetics, and the maximum migration in acetic acid was 1.82 μg/g.

In conclusion, the one-pot polycondensation approach can be used to simultaneously achieve chain extension and nano composition. The successful preparation of PEF/TiO_2 nanocomposites with anti-ultraviolet, anti-blue-light and antibacterial functions also has certain significance for expanding the application range of PEF. The results obtained in this study provide a basis for the continuation of research in the future, which will be related to the packaging application made from PEF of real food and cosmetics, they are likely to have higher requirements for the antibacterial and UV shielding properties of packaging materials to obtain longer storage times in the future.

Declaration of Competing Interest

The authors declare that they have no known competing financial interests or personal relationships that could have appeared to influence the work reported in this paper.

Acknowledgments

This work was supported by the National Natural Science Foundation of China (grant numbers 52273098, 52073284).

Appendix A. Supplementary material

Supplementary data to this article can be found online at https://doi.org/10.1016/j.arabjc.2023.105228.

References

Achilias, D.S., Chondroyiannis, A., Nerantzaki, M., Adam, K.-V., Terzopoulou, Z., Papageorgiou, G.Z., Bikiaris, D.N., 2017. Solid state polymerization of poly (ethylene furanoate) and its nanocomposites with SiO_2 and TiO_2. Macromol. Mater. Eng. 302. https://doi.org/10.1002/mame.201700012.

Alizadeh-Sani, M., Mohammadian, E., McClements, D.J., 2020. Eco-friendly active packaging consisting of nanostructured biopolymer matrix reinforced with TiO_2 and essential oil: Application for preservation of refrigerated meat. Food Chem. 322,. https://doi.org/10.1016/j.foodchem.2020.126782 126782.

Al-Tayyar, N.A., Youssef, A.M., Al-Hindi, R., 2020. Antimicrobial food packaging based on sustainable bio-based materials for reducing foodborne pathogens: A review. Food Chem. 310,. https://doi.org/10.1016/j.foodchem.2019.125915 125915.

Al-Zubaydi, A.S.J., Salih, R.M., Al-Dabbagh, B.M., 2020. Effect of nano TiO_2 particles on the properties of carbon fiber-epoxy composites. Prog. Rubber Plast. Recycl. Technol. 37, 216–232. https://doi.org/10.1177/1477760620977502.

Awaja, F., Pavel, D., 2005. Injection stretch blow moulding process of reactive extruded recycled PET and virgin PET blends. Eur. Polym. J. 41, 2614–2634. https://doi.org/10.1016/j.eurpolymj.2005.05.036.

Azarakhsh, S., Bahiraei, H., Haidari, G., 2022. Electrospun synthesis of silver/poly (vinyl alcohol) nano-fibers: Investigation of microstructure and antibacterial activity. Mater. Lett. 309. https://doi.org/10.1016/j.matlet.2021.131370.

Bouadjela, S., Abdoune, F.Z., Benmoussa, N., Mechernene, L., Rahmoun, K., Maschke, U., 2017. Effect of titanium dioxide nanoparticles on polymer network formation. Spectrosc. Lett. 50, 522–527. https://doi.org/10.1080/00387010.2017.1378683.

Can, U., Kaynak, C., 2019. Effects of micro-nano titania contents and maleic anhydride compatibilization on the mechanical performance of polylactide. Polym. Compos. 41, 600–613. https://doi.org/10.1002/pc.25391.

Can, U., Kaynak, C., 2020. Performance of polylactide against UV irradiation: Synergism of an organic UV absorber with micron and nano-sized TiO_2. J. Compos. Mater. 54, 2489–2504. https://doi.org/10.1177/0021998319899140.

Chen, J., Zhang, X., Bi, F., Zhang, X., Yang, Y., Wang, Y., 2020a. A facile synthesis for uniform tablet-like TiO2/C derived from Materials of Institut Lavoisier-125(Ti) (MIL-125(Ti)) and their enhanced visible light-driven photodegradation of tetracycline. J. Colloid Interface Sci. 571, 275–284. https://doi.org/10.1016/j.jcis.2020.03.055.

Chen, J., Zhang, X., Shi, X., Bi, F., Yang, Y., Wang, Y., 2020b. Synergistic effects of octahedral TiO2-MIL-101(Cr) with two heterojunctions for enhancing visible-light photocatalytic degradation of liquid tetracycline and gaseous toluene. J. Colloid Interface Sci. 579, 37–49. https://doi.org/10.1016/j.jcis.2020.06.042.

Codou, A., Guigo, N., van Berkel, J.G., de Jong, E., Sbirrazzuoli, N., 2017. Preparation and crystallization behavior of poly(ethylene 2,5-furandicarboxylate)/cellulose composites by twin screw extrusion. Carbohydr. Polym. 174, 1026–1033. https://doi.org/10.1016/j.carbpol.2017.07.006.

Connolly, M., Zhang, Y., Brown, D.M., Ortuño, N., Jordá-Beneyto, M., Stone, V., Fernandes, T.F., Johnston, H.J., 2019. Novel polylactic acid (PLA)-organoclay nanocomposite bio-packaging for the cosmetic industry; migration studies and in vitro assessment of the dermal toxicity of migration extracts. Polym. Degrad. Stab. 168. https://doi.org/10.1016/j.polymdegradstab.2019.108938.

Farhoodi, M., Mousavi, S.M.A., Sotudeh-Gharebagh, R., Emam-Djomeh, Z., Oromiehie, A., 2013. Effect of spherical and platelet-like nanoparticles on physical and mechanical properties of polyethylene terephthalate. J. Thermoplast. Compos. Mater. 27, 1127–1138. https://doi.org/10.1177/0892705712475007.

Gomez-Hermoso-de-Mendoza, J., Gutierrez, J., Tercjak, A., 2020. Transparent and flexible cellulose triacetate–TiO_2 nanoparticles with conductive and UV-shielding properties. J. Phys. Chem. C 124, 4242–4251. https://doi.org/10.1021/acs.jpcc.9b11298.

He, Q., Zhang, Y., Cai, X., Wang, S., 2016. Fabrication of gelatin-TiO_2 nanocomposite film and its structural, antibacterial and physical properties. Int. J. Biol. Macromol. 84, 153–160. https://doi.org/10.1016/j.ijbiomac.2015.12.012.

Hu, D., Zhang, Z., Liu, M., Lin, J., Chen, X., Ma, W., 2019a. Multifunctional UV-shielding nanocellulose films modified with halloysite nanotubes-zinc oxide nanohybrid. Cellul. 27, 401–413. https://doi.org/10.1007/s10570-019-02796-0.

Hu, H., Zhang, R., Jiang, Y., Shi, L., Wang, J., Ying, W.B., Zhu, J., 2019b. Toward biobased, biodegradable, and smart barrier packaging material: Modification of poly(Neopentyl Glycol 2,5-Furandicarboxylate) with succinic acid. ACS Sustain. Chem. Eng. 7, 4255–4265. https://doi.org/10.1021/acssuschemeng.8b05990.

Huang, G., Huang, Y., Xu, W., Yao, Q., Liu, X., Ding, C., Chen, X., 2019. Cesium lead halide perovskite nanocrystals for ultraviolet and blue light blocking. Chin. Chem. Lett. 30, 1021–1023. https://doi.org/10.1016/j.cclet.2018.12.028.

Karthikeyan, B., Hariharan, S., Sasidharan, A., Gayathri, V., Arun, T., Akbari-Fakhrabadi, A., Madhumitha, C., 2019. Optical, vibrational and fluorescence recombination pathway properties of nano SiO_2-PVA composite films. Opt. Mater. 90, 139–144. https://doi.org/10.1016/j.optmat.2019.01.063.

Kaur, R., Thakur, N.S., Chandna, S., Bhaumik, J., 2021. Sustainable lignin-based coatings doped with titanium dioxide nanocomposites exhibit synergistic microbicidal and UV-blocking performance toward personal protective equipment. ACS Sustain. Chem. Eng. 9, 11223–11237. https://doi.org/10.1021/acssuschemeng.1c03637.

Kim, J.S., Kuk, E., Yu, K.N., Kim, J.H., Park, S.J., Lee, H.J., Kim, S.H., Park, Y.K., Park, Y.H., Hwang, C.Y., Kim, Y.K., Lee, Y.S., Jeong, D.H., Cho, M.H., 2007. Antimicrobial effects of silver nanoparticles. Nanomedicine 3, 95–101. https://doi.org/10.1016/j.nano.2006.12.001.

Kite, S.V., Kadam, A.N., Sathe, D.J., Patil, S., Mali, S.S., Hong, C.K., Lee, S.W., Garadkar, K.M., 2021. Nanostructured TiO_2 sensitized with MoS_2 nanoflowers for enhanced photodegradation efficiency toward Methyl Orange. ACS Omega 6, 17071–17085. https://doi.org/10.1021/acsomega.1c02194.

Koltsakidou, A., Terzopoulou, Z., Kyzas, G., Bikiaris, D., Lambropoulou, D., 2019. Biobased poly(ethylene furanoate) polyester/TiO2 supported nanocomposites as effective photocatalysts for anti-inflammatory/analgesic drugs. Molecules 24. https://doi.org/10.3390/molecules24030564.

Kourtidou, D., Karfaridis, D., Kehagias, T., Vourlias, G., Bikiaris, D.N., Chrissafis, K., 2023. Incorporating graphene nanoplatelets and carbon nanotubes in biobased poly(ethylene 2,5-furandicarboxylate): Fillers' effect on the matrix's structure and lifetime. Polymers 15. https://doi.org/10.3390/polym15020401.

Li, B., Wang, Z.W., Lin, Q.B., Hu, C.Y., 2016. Study of the migration of stabilizer and plasticizer from polyethylene terephthalate into food simulants. J. Chromatogr. Sci. 54, 939–951. https://doi.org/10.1093/chromsci/bmw025.

Li, L. H. K. T. S. K. G., 2006. Crystallization Characteristics Of Pet/TiO_2 Nanocomposites. Materials Science: An Indian Journal. 2, 154-160.

Lian, Z., Zhang, Y., Zhao, Y., 2016. Nano-TiO_2 particles and high hydrostatic pressure treatment for improving functionality of polyvinyl alcohol and chitosan composite films and nano-TiO_2 migration from film matrix in food simulants. Innov. Food Sci. Emerg. Technol. 33, 145–153. https://doi.org/10.1016/j.ifset.2015.10.008.

Liu, F., Hu, C.Y., Zhao, Q., Shi, Y.J., Zhong, H.N., 2016. Migration of copper from nanocopper/LDPE composite films. Food Addit. Contam. Part A Chem. Anal. Control Expo. Risk Assess. 33, 1741–1749. https://doi.org/10.1080/19440049.2016.1237779.

Loos, K., Zhang, R., Pereira, I., Agostinho, B., Hu, H., Maniar, D., Sbirrazzuoli, N., Silvestre, A.J.D., Guigo, N., Sousa, A.F., 2020. A perspective on PEF synthesis, properties, and end-life. Front. Chem. 8, 585. https://doi.org/10.3389/fchem.2020.00585.

Lotti, N., Munari, A., Gigli, M., Gazzano, M., Tsanaktsis, V., Bikiaris, D.N., Papageorgiou, G.Z., 2016. Thermal and structural response of in situ prepared biobased poly(ethylene 2,5-furan dicarboxylate) nanocomposites. Polymer 103, 288–298. https://doi.org/10.1016/j.polymer.2016.09.050.

Luo, F., Chen, Z., Chen, J., Liu, P., Ding, Y., Zhang, S., Gao, C., Yang, M., 2022. Nanoparticle layer via UV-induced directional migration of iron-doped titania nanoparticles in polyvinyl butyral films and superior UV-stability. Polymer 254. https://doi.org/10.1016/j.polymer.2022.125107.

Luo, Y.-B., Li, W.-D., Wang, X.-L., Xu, D.-Y., Wang, Y.-Z., 2009. Preparation and properties of nanocomposites based on poly(lactic acid) and functionalized TiO_2. Acta Mater. 57, 3182–3191. https://doi.org/10.1016/j.actamat.2009.03.022.

Luyt, A.S., Gasmi, S., 2017. Influence of TiO_2 nanoparticles on the crystallization behaviour and tensile properties of biodegradable PLA and PCL nanocomposites. J. Polym. Environ. 26, 2410–2423. https://doi.org/10.1007/s10924-017-1142-y.

Martino, L., Guigo, N., van Berkel, J.G., Sbirrazzuoli, N., 2017. Influence of organically modified montmorillonite and sepiolite clays on the physical properties of bio-based poly(ethylene 2,5-furandicarboxylate). Compos. B Eng. 110, 96–105. https://doi.org/10.1016/j.compositesb.2016.11.008.

Menager, C., Guigo, N., Martino, L., Sbirrazzuoli, N., Visser, H., Boyer, S.A.E., Billon, N., Monge, G., Combeaud, C., 2018. Strain induced crystallization in biobased Poly (ethylene 2,5-furandicarboxylate) (PEF); conditions for appearance and microstructure analysis. Polymer 158, 364–371. https://doi.org/10.1016/j.polymer.2018.10.054.

Mesgari, M., Aalami, A.H., Sahebkar, A., 2021. Antimicrobial activities of chitosan/titanium dioxide composites as a biological nanolayer for food preservation: A review. Int. J. Biol. Macromol. 176, 530–539. https://doi.org/10.1016/j.ijbiomac.2021.02.099.

Nakazato, G., Kobayashi, R.K.T., Seabra, A.B., Duran, N., 2017. Use of nanoparticles as a potential antimicrobial for food packaging. Food Preserv., 413–447

Nikam, P.N., Deshpande, V.D., 2019. Isothermal crystallization kinetics of PET/alumina nanocomposites using distinct macrokinetic models. J. Therm. Anal. Calorim. 138, 1049–1067. https://doi.org/10.1007/s10973-019-08192-x.

Nikolic, M.V., Vasiljevic, Z.Z., Auger, S., Vidic, J., 2021. Metal oxide nanoparticles for safe active and intelligent food packaging. Trends Food Sci. Technol. 116, 655–668. https://doi.org/10.1016/j.tifs.2021.08.019.

Pandey, V., Seese, M., Maia, J.M., Schiraldi, D.A., 2020. Thermo-rheological analysis of various chain extended recycled poly(ethylene terephthalate). Polym. Eng. Sci. 60, 2511–2516. https://doi.org/10.1002/pen.25488.

Papageorgiou, G.Z., Nikolaidis, G.N., Ioannidis, R.O., Rinis, K., Papageorgiou, D.G., Klonos, P.A., Achilias, D.S., Kapnisti, M., Terzopoulou, Z., Bikiaris, D.N., 2022. A step forward in thermoplastic polyesters: Understanding the crystallization and melting of biobased poly(ethylene 2,5-furandicarboxylate) (PEF). ACS Sustain. Chem. Eng. 10, 7050–7064. https://doi.org/10.1021/acssuschemeng.2c00995.

Sadowski, R., Wach, A., Buchalska, M., Kuśtrowski, P., Macyk, W., 2019. Photosensitized TiO_2 films on polymers-Titania-polymer interactions and

visible light induced photoactivity. Appl. Surf. Sci. 475, 710–719. https://doi.org/10.1016/j.apsusc.2018.12.286.
Salomatina, E.V., Loginova, A.S., Ignatov, S.K., Knyazev, A.V., Spirina, I.V., Smirnova, L. A., 2016. Structure and catalytic activity of poly(Titanium Oxide) doped by gold nanoparticles in organic polymeric matrix. J. Inorg. Organomet. Polym Mater. 26, 1280–1291. https://doi.org/10.1007/s10904-016-0409-4.
Silva-Leyton, R., Quijada, R., Bastías, R., Zamora, N., Olate-Moya, F., Palza, H., 2019. Polyethylene/graphene oxide composites toward multifunctional active packaging films. Compos. Sci. Technol. 184. https://doi.org/10.1016/j.compscitech.2019.107888.
Siripatrawan, U., Kaewklin, P., 2018. Fabrication and characterization of chitosan-titanium dioxide nanocomposite film as ethylene scavenging and antimicrobial active food packaging. Food Hydrocoll. 84, 125–134. https://doi.org/10.1016/j.foodhyd.2018.04.049.
Sousa, A.F., Patrício, R., Terzopoulou, Z., Bikiaris, D.N., Stern, T., Wenger, J., Loos, K., Lotti, N., Siracusa, V., Szymczyk, A., Paszkiewicz, S., Triantafyllidis, K.S., Zamboulis, A., Nikolic, M.S., Spasojevic, P., Thiyagarajan, S., van Es, D.S., Guigo, N., 2021. Recommendations for replacing PET on packaging, fiber, and film materials with biobased counterparts. Green Chem. 23, 8795–8820. https://doi.org/10.1039/d1gc02082j.
Sousa, A.F., Silvestre, A.J.D., 2022. Plastics from renewable sources as green and sustainable alternatives. Curr. Opin. Green Sustainable Chem. 33. https://doi.org/10.1016/j.cogsc.2021.100557.
Stoclet, G., Gobius du Sart, G., Yeniad, B., de Vos, S., Lefebvre, J.M., 2015. Isothermal crystallization and structural characterization of poly(ethylene-2,5-furanoate). Polymer 72, 165–176. https://doi.org/10.1016/j.polymer.2015.07.014.
Sun, L., Wang, J., Mahmud, S., Jiang, Y., Zhu, J., Liu, X., 2019. New insight into the mechanism for the excellent gas properties of poly(ethylene 2,5-furandicarboxylate) (PEF): Role of furan ring's polarity. Eur. Polym. J. 118, 642–650. https://doi.org/10.1016/j.eurpolymj.2019.06.033.
Tang, H., Dong, Q., Liu, P., Ding, Y., Wang, F., Gao, C., Zhang, S., Yang, M., 2016. Isothermal crystallization of polypropylene/surface modified silica nanocomposites. Sci. China Chem. 59, 1283–1290. https://doi.org/10.1007/s11426-016-0146-0.
Tang, Z., Fan, F., Fan, C., Jiang, K., Qin, Y., 2020. The performance changes and migration behavior of PLA/Nano-TiO_2 composite film by high-pressure treatment in ethanol solution. Polymers (Basel). 12. https://doi.org/10.3390/polym12020471.
van Berkel, J.G., Guigo, N., Kolstad, J.J., Sipos, L., Wang, B., Dam, M.A., Sbirrazzuoli, N., 2015. Isothermal crystallization kinetics of poly (ethylene 2,5-furandicarboxylate). Macromol. Mater. Eng. 300, 466–474. https://doi.org/10.1002/mame.201400376.
Vassiliou, A., Bikiaris, D., Chrissafis, K., Paraskevopoulos, K.M., Stavrev, S.Y., Docoslis, A., 2008. Nanocomposites of isotactic polypropylene with carbon nanoparticles exhibiting enhanced stiffness, thermal stability and gas barrier properties. Compos. Sci. Technol. 68, 933–943. https://doi.org/10.1016/j.compscitech.2007.08.019.
Vejdan, A., Ojagh, S.M., Adeli, A., Abdollahi, M., 2016. Effect of TiO_2 nanoparticles on the physico-mechanical and ultraviolet light barrier properties of fish gelatin/agar bilayer film. LWT Food Sci. Technol. 71, 88–95. https://doi.org/10.1016/j.lwt.2016.03.011.
Wang, J., Liu, X., Zhang, Y., Liu, F., Zhu, J., 2016. Modification of poly(ethylene 2,5-furandicarboxylate) with 1,4-cyclohexanedimethylene: Influence of composition on mechanical and barrier properties. Polymer 103, 1–8. https://doi.org/10.1016/j.polymer.2016.09.030.
Wang, J., Liu, X., Jia, Z., Liu, Y., Sun, L., Zhu, J., 2017a. Synthesis of bio-based poly (ethylene 2,5-furandicarboxylate) copolyesters: Higher glass transition temperature, better transparency, and good barrier properties. J. Polym. Sci. A Polym. Chem. 55, 3298–3307. https://doi.org/10.1002/pola.28706.
Wang, J., Liu, X., Zhu, J., Jiang, Y., 2017b. Copolyesters based on 2,5-furandicarboxylic acid (FDCA): Effect of 2,2,4,4-Tetramethyl-1,3-Cyclobutanediol units on their properties. Polymers (Basel) 9. https://doi.org/10.3390/polym9090305.
Wang, Z., Xiang, M., Huo, B., Wang, J., Yang, L., Ma, W., Qi, J., Wang, Y., Zhu, Z., Meng, F., 2023b. A novel ZnO/CQDs/PVDF piezoelectric system for efficiently degradation of antibiotics by using water flow energy in pipeline: Performance and mechanism. Nano Energy 107. https://doi.org/10.1016/j.nanoen.2022.108162.
Wang, J., Zhou, X., Hao, J., Wang, Z., Huo, B., Qi, J., Wang, Y., Meng, F., 2023a. Sustainable self-powered degradation of antibiotics using Fe3O4@MoS2/PVDF modified pipe with superior piezoelectric activity: Mechanism insight, toxicity assessment and energy consumption. Appl. Catal. B:Environ. 331. https://doi.org/10.1016/j.apcatb.2023.122655.
Watté, J., Van Gompel, W., Lommens, P., De Buysser, K., Van Driessche, I., 2016. Titania nanocrystal surface functionalization through silane chemistry for low temperature deposition on polymers. ACS Appl. Mater. Interfaces 8, 29759–29769. https://doi.org/10.1021/acsami.6b08931.
Wu, W., Liu, T., Deng, X., Sun, Q., Cao, X., Feng, Y., Wang, B., Roy, V.A.L., Li, R.K.Y., 2019. Ecofriendly UV-protective films based on poly(propylene carbonate) biocomposites filled with TiO_2 decorated lignin. Int. J. Biol. Macromol. 126, 1030–1036. https://doi.org/10.1016/j.ijbiomac.2018.12.273.
Xie, H., Meng, H., Wu, L., Li, B.-G., Dubois, P., 2019. In-situ synthesis, thermal and mechanical properties of biobased poly(ethylene 2,5-furandicarboxylate)/montmorillonite (PEF/MMT) nanocomposites. Eur. Polym. J. 121. https://doi.org/10.1016/j.eurpolymj.2019.109266.
Xie, H., Wu, L., Li, B.-G., Dubois, P., 2020. Modification of poly(ethylene 2,5-furandicarboxylate) with aliphatic polycarbonate diols: 1. Randomnized copolymers with significantly improved ductility and high CO_2 barrier performance. Eur. Polym. J. 134. https://doi.org/10.1016/j.eurpolymj.2020.109856.
Xu, W., Zhong, L., Xu, F., Song, W., Wang, J., Zhu, J., Chou, S., 2019. Ultraflexible transparent bio-based polymer conductive films based on Ag nanowires. Small 15, e1805094.
Yang, Y., Ju, Y., Li, Y., Yin, L., Chen, L., Gu, P., Zhang, J., 2020. Transparent nanostructured BiVO4 double films with blue light shielding capabilities to prevent damage to ARPE-19 cells. ACS Appl. Mater. Interfaces 12, 20797–20805. https://doi.org/10.1021/acsami.9b22465.
Yang, Y., Zhao, S., Bi, F., Chen, J., Li, Y., Cui, L., Xu, J., Zhang, X., 2022a. Oxygen-vacancy-induced O2 activation and electron-hole migration enhance photothermal catalytic toluene oxidation. Cell Rep. Phys. Sci. 3. https://doi.org/10.1016/j.xcrp.2022.101011.
Yang, Y., Zhao, S., Bi, F., Chen, J., Wang, Y., Cui, L., Xu, J., Zhang, X., 2022b. Highly efficient photothermal catalysis of toluene over Co3O4/TiO2 p-n heterojunction: The crucial roles of interface defects and band structure. Appl. Catal. B:Environ. 315. https://doi.org/10.1016/j.apcatb.2022.121550.
Youssef, A.M., Abd El-Aziz, M.E., Morsi, S.M.M., 2022. Development and evaluation of antimicrobial LDPE/TiO_2 nanocomposites for food packaging applications. Polym. Bull. 80, 5417–5431. https://doi.org/10.1007/s00289-022-04346-4.
Zhang, Q., Jiang, M., Wang, G., Zhou, G., 2020. Novel biobased high toughness PBAT/PEF blends: morphology, thermal properties, crystal structures and mechanical properties. New J. Chem. 44, 3112–3121. https://doi.org/10.1039/c9nj04861h.
Zhang, W., Jiang, H., Rhim, J.W., Cao, J., Jiang, W., 2022a. Effective strategies of sustained release and retention enhancement of essential oils in active food packaging films/coatings. Food Chem. 367,. https://doi.org/10.1016/j.foodchem.2021.130671 130671.
Zhang, W., Rhim, J.-W., 2022. Titanium dioxide (TiO_2) for the manufacture of multifunctional active food packaging films. Food Packag. Shelf Life 31. https://doi.org/10.1016/j.fpsl.2021.100806.
Zhang, Q., Song, M., Xu, Y., Wang, W., Wang, Z., Zhang, L., 2021. Bio-based polyesters: Recent progress and future prospects. Prog. Polym. Sci. 120. https://doi.org/10.1016/j.progpolymsci.2021.101430.
Zhang, X., Zhao, Z., Zhao, S., Xiang, S., Gao, W., Wang, L., Xu, J., Wang, Y., 2022b. The promoting effect of alkali metal and H_2O on Mn-MOF derivatives for toluene oxidation: A combined experimental and theoretical investigation. J. Catal. 415, 218–235. https://doi.org/10.1016/j.jcat.2022.10.005.
Zhang, X., Zhu, Z., Rao, R., Chen, J., Han, X., Jiang, S., Yang, Y., Wang, Y., Wang, L., 2022c. Highly efficient visible-light-driven photocatalytic degradation of gaseous toluene by rutile-anatase TiO2@MIL-101 composite with two heterojunctions. J. Environ. Sci. https://doi.org/10.1016/j.jes.2022.03.014.
Zhou, G., Li, L., Jiang, M., Wang, G., Wang, R., Wu, G., Zhou, G., 2021. Renewable poly (butene 2, 5-furan dicarboxylate) nanocomposites constructed by TiO_2 nanocubes: Synthesis, crystallization, and properties. Polym. Degrad. Stab. 189. https://doi.org/10.1016/j.polymdegradstab.2021.109591.
Zhu, Z., Cai, H., Sun, D.-W., 2018. Titanium dioxide (TiO_2) photocatalysis technology for nonthermal inactivation of microorganisms in foods. Trends Food Sci. Technol. 75, 23–35. https://doi.org/10.1016/j.tifs.2018.02.018.
Zibaei, R., B. Ebrahimi, M. Rouhi, Z. Hashami, Z. Roshandel, S. Hasanvand, J. de Toledo Guimarães, M. goharifar & R. Mohammadi, 2023. Development of packaging based on PLA/POE/SeNPs nanocomposites by blown film extrusion method: Physicochemical, structural, morphological and antioxidant properties. Food Packaging and Shelf Life. 38. https://doi.org/10.1016/j.fpsl.2023.101104.